Inorganic Chemistry
Article

*Inorg. Chem.* **2009**, *48*, 11697–11711 **11697**
DOI: 10.1021/ic901744m

# Synthesis, Structure, and Transformation Studies in a Family of Inorganic−Organic Hybrid Framework Structures Based on Indium

**Padmini Ramaswamy,[†] Nayana N. Hegde,[†] Ramanath Prabhu,[†] V. M. Vidya,[†] Ayan Datta,[‡] and Srinivasan Natarajan*[,†]**

[†]*Framework Solids Laboratory, Solid State and Structural Chemistry Unit, Indian Institute of Science, Bangalore 560012, India and* [‡]*School of Chemistry, Indian Institute of Science Education and Research (IISER), Thiruvananthapuram, CET Campus, Thiruvananthapuram - 695016, Kerala, India*

Received September 2, 2009

Eight new open-framework inorganic−organic hybrid compounds based on indium have been synthesized employing hydrothermal methods. All of the compounds have $InO_6$, $C_2O_4$, and $HPO_3/HPO_4/SO_4$ units connected to form structures of different dimensionality. Thus, the compounds have zero- (**I**), two- (**II**, **III**, **IV**, **V**, **VII**, and **VIII**), and three-dimensionally (**VI**) extended networks. The formation of the first zero-dimensional hybrid compound is noteworthy. In addition, concomitant polymorphic structures have been observed in the present study. The molecular compound, **I**, was found to be reactive, and the transformation studies in the presence of a base (pyridine) give rise to the polymorphic structures of **II** and **III**, while the addition of an acid ($H_3PO_3$) gives rise to a new indium phosphite with a pillared layer structure (**T1**). Preliminary density functional theory calculations suggest that the stabilities of the polymorphs are different, with one of the forms (**II**) being preferred over the other, which is consistent with the observed experimental behavior. The oxalate units perform more than one role in the present structures. Thus, the oxalate units connect two In centers to satisfy the coordination requirements as well as to achieve charge balance in compounds **II**, **IV**, and **VI**. The terminal oxalate units observed in compounds **I**, **IV**, and **V** suggest the possibility of intermediate structures. Both *in-plane* and *out-of-plane* connectivity of the oxalate units were observed in compound **VI**. The compounds have been characterized by powder X-ray diffraction, IR spectroscopy, thermogravimetric analysis, and $^{31}P$ NMR studies.

## Introduction

The many potential applications in the areas of catalysis, sorption, and separation processes are the reasons for continuing interest in open-framework inorganic−organic hybrid compounds.[1,2] The aluminosilicates are the most widely studied family of framework structured compounds.[3] The discovery of aluminophosphates with comparable structures to the aluminosilicate zeolites during the early 1980s really opened this area for active research.[4] Persistent research efforts over the years have established that the family of framework compounds incorporates a majority of the metals of the periodic table.[2,3] It has been possible to show that other related anions such as arsenates,[2] sulfates,[5] and so forth also form interesting open structures.

During the past decade or so, it became apparent that the phosphite group, $[HPO_3]^{2-}$, which is closely related to the phosphate group, $(PO_4)^{3-}$, can also be incorporated as part of the framework structure. The phosphite group provides subtle differences compared to the phosphate units due to the following reasons: (i) the phosphite group offers three P−O bonds compared to four in the phosphates, and (ii) the average charge on the P−O bond in the phosphite group is less (0.67) compared to the phosphate (0.75). The combined effects of the reduced charge and the possible binding sites (P−O bonds) in the phosphite group, however, could be fruitfully exploited to design and form newer structures (topologies) that may not be feasible in the phosphate structures. A careful scrutiny of the available literature clearly reveals that the phosphite group can also give rise to structures of considerable diversity. Thus, phosphite frameworks of Zn,[6] Fe,[7] V,[8] Co,[9] and Cr[10] have been synthesized and characterized. Though the phosphites have comparable

*E-mail: snatarajan@sscu.iisc.ernet.in.

(1) Maspoch, D.; Ruiz-Molina, D.; Veciana, J. *Chem. Soc. Rev.* **2007**, *36*, 770.
(2) Natarajan, S.; Mandal, S. *Angew. Chem., Int. Ed.* **2008**, *47*, 4798.
(3) Cheetham, A. K.; Loiseau, T.; Ferey, G. *Angew. Chem., Int. Ed.* **1999**, *38*, 3268.
(4) Wilson, S. T.; Lok, B. M.; Messina, C. A.; Cannan, T. R.; Flanigen, E. M. *J. Am. Chem. Soc.* **1982**, *104*, 1146.
(5) Rao, C. N. R.; Behera, J. N.; Dan, M. *Chem. Soc. Rev.* **2006**, *35*, 375.
(6) (a) Gordon, L. E.; Harrison, W. T. A. *Inorg. Chem.* **2004**, *43*, 1808. (b) Mandal, S.; Natarajan, S. *Inorg. Chem.* **2008**, *47*, 5304.
(7) (a) Fernandez, S.; Mesa, J. L.; Pizarro, J. L.; Garitaonandia, J. S.; Arriortua, M. I.; Rojo, T. *Angew. Chem., Int. Ed.* **2004**, *43*, 977. (b) Chung, U.-C.; Mesa, J. L.; Pizarro, J. L.; Fernandez, J. R.; Marcos, J. S.; Garitaonandia, J. S.; Arriortua, M. I.; Rojo, T. *Inorg. Chem.* **2006**, *45*, 8965.
(8) (a) Fernandez, S.; Mesa, J. L.; Pizarro, J. L.; Lezama, L.; Arriortua, M. I.; Rojo, T. *Chem. Mater.* **2002**, *14*, 2300. (b) Zhang, D.; Yue, H.; Shi, Z.; Guo, M.; Feng, S. *Microporous Mesoporous Mater.* **2005**, *82*, 209.


Published on Web 11/13/2009

**Table 1.** Synthesis Conditions for Compounds **I**−**VIII**

| synthesis condition | | | | | composition | |
|---|---|---|---|---|---|---|
| mole ratio | pH (initial) | pH (final) | temp (°C) | time (h) | yield (%) | |
| 1.0 $In_2(SO_4)_3$/6.8 $H_3PO_3$/8.0 $H_2C_2O_4$/20.0 pip/1110 $H_2O$ | 4.0 | 4.0 | 110 | 48 | 85 | $[C_4N_2H_{12}]_3[In_2(HPO_3)_2(C_2O_4)_4]\cdot 4H_2O$, **I** |
| 1.0 $In_2(SO_4)_3$/3.6 $H_3PO_3$/2.6 $H_2C_2O_4$/32.0 py/10.4 HF/1.0 1,4-DAB/95 $H_2O$ | 6.5 | 4.0 | 180 | 72 | 85 + 15 | $[In_2(HPO_3)_2(C_2O_4)(C_5H_5N)_2]$, **II**+ **III** |
| 1.0 $In_2(SO_4)_3$/3.6 $H_3PO_3$/2.6 $H_2C_2O_4$/32.0 py/10.4 HF/95 $H_2O$ | 6.5 | 4.0 | 180 | 72 | 90 | $[In_2(HPO_3)_2(C_2O_4)(C_5H_5N)_2]$, pure phase of **II** |
| 1.0 $InCl_3$/1.7 $H_3PO_3$/2.0 $H_2C_2O_4$/4.0 pip/278 $H_2O$ | 4.0 | 4.0 | 180 | 72 | 75 | $[C_4N_2H_{12}]_2[In_2(HPO_3)_3(C_2O_4)_2]\cdot 3H_2O$, **IV** |
| 1.0 $In_2(SO_4)_3$/6.8 $H_3PO_3$/8.0 $H_2C_2O_4$/20.0 pip/1110 $H_2O$ | 4.0 | 4.0 | 180 | 48 | 75 | $[C_4N_2H_{12}]_3[In_4(HPO_3)_6(C_2O_4)_3]$, **V** |
| 1.0 $InCl_3$/4.0 $H_3PO_3$/9.0 $H_2C_2O_4$/5.0 1,4-DAB/1630 $H_2O$ | 2.0 | 2.0 | 125 + 150 | 48 + 72 | 80 | $[C_4N_2H_{14}][In_4(H_2O)(HPO_3)_5(C_2O_4)_2]\cdot 2H_2O$, **VI** |
| 1.0 $In_2(SO_4)_3$/3.0 $H_2C_2O_4$/2.0 pip/445 $H_2O$ | 2.0 | 2.0 | 110 + 150 | 48 + 48 | 85 | $[C_4N_2H_{12}]_{0.5}[In(SO_4)(C_2O_4)]\cdot H_2O$, **VII** |
| 1.0 $InCl_3$/4.0 $H_3PO_4$/9.0 $H_2C_2O_4$/5.0 pip/1630 $H_2O$ | 2.0 | 2.0 | 110 + 150 | 48 + 24 | 70 | $[C_4N_2H_{12}]_{0.5}[In(HPO_4)(C_2O_4)]\cdot H_2O$, **VIII** |

structures to those of the phosphates, they also form novel frameworks. Thus, in the iron phosphite, $[C_5H_{18}N_3][Fe_3(HPO_3)_6]\cdot 3H_2O$,[7b] the framework closely resembles the NASICON[11] structure. A new pentameric secondary building unit (SBU) has been observed in the vanadium phosphite, $[C_2N_2H_{10}][(VO)_3(H_2O)(HPO_3)_4]\cdot H_2O$.[8b] The phosphite family has also given rise to the first amine-templated chromium phosphite structure, $[C_2H_{10}N_2][Cr(HPO_3)F_3]$.[10]

One of the important developments in the area of framework compounds is the use of both organic as well as inorganic anions for building open structures. It is expected that the variable nature of the binding properties of the organic and the inorganic moieties could lead to interesting structures. Additionally, the organic anions such as oxalates could be used as rigid pillaring units to bind inorganic layers. Thus, the use of oxalates along with the phosphates and the arsenates has given rise to new types of inorganic−organic hybrid frameworks.[2,12]

In this context, it would be worthwhile to examine the formation of new hybrid frameworks by combining the phosphite and the oxalate units. Our efforts in this direction employing the transition elements have yielded new phosphite−oxalate structures of different dimensionalities.[13] The phosphite−oxalate structures of transition elements appear to have much in common with the phosphate−oxalate frameworks. The research on the phosphate−oxalate structures of the main group elements, though not plentiful, shows interesting structural features.[14] Thus, the aluminum phosphate−oxalate, $[N_2C_4H_{12}][Al_2(PO_4)(HPO_4)(C_2O_4)]\cdot H_2O$,[14b] has one-dimensional chains of double six rings connected by the oxalate units. Similarly, the phosphite−oxalate hybrid structures of the main group elements could also lead to the formation of interesting frameworks. We have been focusing our attention on the main group elements, such as indium, with a view to establishing newer framework structures that would involve both the phosphite and the oxalate units. Our efforts in this direction have been successful, and we have isolated eight new inorganic−organic hybrid compounds. The compounds $[C_4N_2H_{12}]_3[In_2(HPO_3)_2(C_2O_4)_4]\cdot 4H_2O$, **I**; $[In_2(HPO_3)_2(C_2O_4)(C_5H_5N)_2]$, **II** and **III**; $[C_4N_2H_{12}]_2[In_2(HPO_3)_3(C_2O_4)_2]\cdot 3H_2O$, **IV**; $[C_4N_2H_{12}]_3[In_4(HPO_3)_6(C_2O_4)_3]$, **V**; $[C_4N_2H_{14}][In_4(H_2O)(HPO_3)(C_2O_4)_2]\cdot 2H_2O$, **VI**; $[C_4N_2H_{12}]_{0.5}[In(H_2O)(SO_4)(C_2O_4)]\cdot H_2O$, **VII**; and $[C_4N_2H_{12}]_{0.5}[In(H_2O)(HPO_4)(C_2O_4)]\cdot H_2O$, **VIII**, have been obtained by employing hydrothermal methods. The indium phosphite−oxalate compounds exhibit structures that have zero-, two-, and three-dimensionally extended networks. During the present study, the isolations of a zero-dimensional hybrid structure, **I**, and two polymorphic structures, **II** and **III**, are among the first such observations in the family of hybrid compounds. In this paper, we describe the synthesis, structure, and transformation studies of the phosphite−oxalate compounds of indium.

## Experimental Section

The oxalate hybrids of indium **I**−**VIII** were synthesized under hydrothermal conditions starting from a mixture containing the source of indium salt, $H_3PO_3/H_3PO_4$, oxalic acid, and an organic amine. The various synthesis conditions employed in the present study are presented in Table 1. In all of the cases, the reaction mixtures were homogenized for ∼30 min at room temperature and heated in a 23 mL PTFE-lined stainless steel acid digestion bomb (final fill factor ∼40%) at varying times and temperatures. The resulting products, which predominantly contained good-quality, colorless, single crystals, suitable for single-crystal X-ray diffraction, were filtered and washed thoroughly with deionized water. Thus, rod-like (**III**, **VII**, and **VIII**), plate-like (**I**, **II**, and **IV**), and needle-like (**V** and **VI**) crystals were obtained. The polymorphs **II** and **III** crystallized concomitantly during

(9) (a) Armas, S. F.; Mesa, J. L.; Pizarro, J. L.; Chung, U.-C.; Arriortua, M. I.; Rojo, T. *J. Solid State Chem.* **2005**, *178*, 3554. (b) Liu, W.; Chen, H.-H.; Yang, X.-X.; Zhao, J.-T. *Eur. J. Inorg. Chem.* **2005**, *5*, 946.

(10) Fernandez, S.; Mesa, J. L.; Pizarro, J. L.; Lezama, L.; Arriortua, M. I.; Rojo, T *Angew. Chem., Int. Ed.* **2002**, *41*, 3683.

(11) Chakir, M.; Jazouli, A. El.; de Waal, D. *Mater. Res. Bull.* **2003**, *38*, 1773.

(12) (a) Chakrabarti, S.; Natarajan, S. *Angew. Chem., Int. Ed.* **2002**, *41*, 1224. (b) Chakrabarti, S.; Green, M. A.; Natarajan, S. *Solid State Sci.* **2002**, *4*, 405. (c) Choudhury, A.; Natarajan, S.; Rao, C. N. R. *Chem.—Eur. J.* **2000**, *6*, 1168. (d) Meng, H.; Li, G.-H; Xing, Y.; Yang, Y.-L.; Cui, Y.-J.; Liu, L.; Ding, H.; Pang, W.-Q. *Polyhedron* **2004**, *23*, 2357. (e) Jiang, Y.-C.; Wang, S.-L.; Lii, K.-H; Nguyen, N.; Ducouret, A. *Chem. Mater.* **2003**, *15*, 1633. (f) Tang, M.-F.; Lii, K.-H. *J. Solid State Chem.* **2004**, *177*, 1912.

(13) (a) Mandal, S.; Natarajan, S. *Chem.—Eur. J.* **2007**, *13*, 968. (b) Mandal, S.; Green, M. A.; Pati, S. K.; Natarajan, S. *J. Mater. Chem.* **2007**, *17*, 980. (c) Mandal, S.; Pati, S. K.; Green, M. A.; Natarajan, S. *Chem. Mater.* **2005**, *17*, 2912.

(14) (a) Lightfoot, P.; Lethbridge, Z. A. D.; Morris, R. E.; Wragg, D. S.; Wright, P. A.; Kvick, A.; Vaughan, G. B. M. *J. Solid State Chem.* **1999**, *143*, 74–76. (b) Kedarnath, K.; Choudhury, A.; Natarajan, S. *J. Solid State Chem.* **2000**, *150*, 324. (c) Huang, Y.-F.; Lii, K.-H. *J. Chem. Soc., Dalton Trans.* **1998**, *24*, 4085.

the course of a hydrothermal reaction. While polymorph **II** was formed as the major product, **III** occurred in very low yield (< 15%), and hence, other than the single crystal structure studies, we were not able to characterize this compound satisfactorily.

Initial characterizations were carried out by elemental analysis, powder X-ray diffraction (XRD), thermogravimetric analysis (TGA), and IR spectroscopic studies. Elemental analysis of the crystals was carried out using a CHNS analyzer (ThermoFinnigan FLASH EA 1112 CHNS analyzer). The results are presented in Table S2 (see the Supporting Information).

The powder XRD patterns were recorded on crushed single crystals in the $2\theta$ range 5−50° using Cu K$\alpha$ radiation (Philips X'pert Pro). The XRD patterns of the compounds **I**, **II**, and **IV**−**VIII** indicated that the products were pure and consistent with the XRD patterns simulated from the single-crystal structure (see Supporting Information Figure S7a and b). The XRD patterns of the two polymorphic phases **II** and **III** appear to be quite similar but show subtle variations (Figure S7c).

TGA studies have been carried out (Mettler-Toledo, TG850) in an oxygen atmosphere (flow rate = 50 mL/min) in the temperature range 25−800 °C (heating rate = 5 °C/min; see Supporting Information, Figure S6). The results indicated a two-step weight loss in the case of compounds **I**, **IV**, and **VII**. The first weight loss (obsd 6.53% for **I**, 5.89% for **IV**, and 9.73% for **VII**) occurring in the region 30−150 °C corresponds to the loss of the lattice water molecules and coordinated water molecules (calcd 6.68% for **I**, 6.17% for **IV**, and 9.50% for **VII**). The second weight loss (obsd 49.92% for **I**, 40.19% for **IV**, 36.58% for **VII**) occurring in the temperature range 220−500 °C corresponds to the loss of the oxalate and the amine molecules (calcd 57.16% for **I**, 48.82% for **IV**, and 34.85% for **VII**). For compounds **II** and **V**, a single continuous weight loss was observed over a broad temperature range of 250−600 °C (obsd 33.39% for **II** and 22.15% for **V**). This weight loss corresponds to the loss of the amine and the oxalate moieties (calcd. 38.70% for **II** and 35.98% for **V**). The TGA curves showed a number of weight losses in a continuous fashion for compounds **VI** and **VIII**, indicating a complex decomposition process (obsd 19.79% for **VI** and 43.88% for **VIII**). The weight loss could be due to the loss of oxalate, amine molecules, and a loss of the lattice and coordinated water molecules (calcd 27.14% for **VI** and 44.35% for **VIII**). From the TGA studies, we observed that the calculated and observed weight losses in **I**−**VI** differ considerably. For **I**, the total calculated weight loss (loss of lattice water, decomposition of oxalate and amine) is 63.84% (obsd 56.45%), for **II** it is 38.70% (obsd 33.39%), for **IV** it is 54.99% (obsd 46.09%), for **V** it is 35.98% (obsd 22.15%), and for **VI** it is 27.14% (obsd 19.79%). The difference between the observed and calculated weight losses can be explained by considering the oxidation of $P^{III}$ to $P^{V}$ during the decomposition process. The calculated weight gain for the oxidation of $P^{III}$ to $P^{V}$ is 4.31% for **I**, 5.03% for **II**, 7.43% for **IV**, 10.64% for **V**, and 7.59% for **VI**. Combining these, the weight losses would be, for **I**, 60.76% {(56.45 + 4.31)} (calcd 63.84%); for II, 38.42% {(33.39 + 5.03)} (calcd 38.70%); for **IV**, 53.52% {(46.09 + 7.43)} (calcd 54.99%); for **V**, 32.79% {(22.15 + 10.64)} (calcd 35.98%); and for **VI**, 27.38%{(19.79. + 7.59)} (calcd 24.84%) and appear to be closer to the expected weight losses. In compounds **I**−**VI** and **VIII**, the final decomposed products were poorly crystalline, and the majority of the X-ray lines correspond to the indium phosphate phase, $InPO_4$ (JCPDS: 08-0052). The decomposition of compound **VII** produced an amorphous residue.

IR spectroscopic studies were carried out in the range 400−4000 $cm^{-1}$ using the KBr pellet method (Perkin-Elmer, SPECTRUM 1000). IR spectroscopic studies exhibited typical peaks corresponding to the amine molecule, the $HPO_3/HPO_4/SO_4$ moiety, and the lattice water molecule with a few variations in their respective bands (see the Supporting Information, Figure S8). IR (KBr): $\nu_s(H_2O)$ = 3515−3525 $cm^{-1}$, $\nu_s$(N−H) = 3015−3350 $cm^{-1}$, $\nu a_s$-(C−H) = 2850−3075 $cm^{-1}$ $\nu_s$(C−H) = 2825−2970 $cm^{-1}$, $\nu_s$(P−H) = 2370−2408 $cm^{-1}$, $\delta_{as}(H_2O)$ = 1620−1642 $cm^{-1}$, $\nu_s$(C−O) = 1655−1690 $cm^{-1}$, $\delta_s$(N−H) = 1515−1605 $cm^{-1}$, $\delta_s$(C−H) = 1460−1480 $cm^{-1}$, $\delta_s$(C−O) = 1405−1430 $cm^{-1}$, $\nu_s$(C−N) = 1100−1160 $cm^{-1}$, $\nu_{as}$(P−O) = 1023−1140 $cm^{-1}$, $\delta_{as}$(P−H) = 985−1050 $cm^{-1}$, $\nu_s$(P−O) = 865−1010 $cm^{-1}$, $\delta_s$(P−O) = 570−610 $cm^{-1}$, $\delta_{as}$(P−O) = 450−500 $cm^{-1}$; in compound **VII**, $\nu_1(SO_4)$ = 980−1010 $cm^{-1}$, $\nu_3(SO_4)$ = 1090−1140 $cm^{-1}$, $\delta(SO_4)$ = 500−700 $cm^{-1}$.

**Solid-State MAS NMR Studies.** Solid-state nuclear magnetic resonance (NMR) experiments were performed on a Bruker AVIII 500 spectrometer operating at 11.7 T with a resonance frequency of 202.47 MHz for $^{31}$P. A Bruker 4 mm cross-polarization magic angle spinning (CPMAS) probe was used for the experiments. The $^{31}$P MAS spectra were recorded using standard cross-polarization procedures and high proton decoupling, employing a magic angle spinning frequency of 10 kHz. In a typical experiment, rf fields of 100 kHz were used, and the chemical shifts are reported relative to 85% $H_3PO_4$ as the external standard.

**Single-Crystal Structure Determination.** A suitable crystal for all compounds was carefully selected under a polarizing microscope and glued to a thin glass fiber. The single-crystal diffraction data were collected on a Bruker AXS Smart Apex CCD diffractometer at 293(2) K. The X-ray generator was operated at 50 kV and 35 mA using Mo K$\alpha$ ($\lambda$ = 0.71073 Å) radiation. Data were collected with a $\omega$ scan width of 0.3°. A total of 606 frames were collected at three different settings of $\varphi$ (0°, 90°, 180°), keeping the sample-to-detector distance fixed at 6.03 cm and the detector position ($2\theta$) fixed at −25°. Pertinent experimental details of the structure determination of **I**−**VIII** are presented in Table 2a and b.

The data were reduced using SAINTPLUS,[15] and an empirical absorption correction was applied using the SADABS program.[16] The crystal structure was solved and refined using SHELXL97 present in the WinGx suit of programs (version 1.63.04a).[17] The hydrogen atom on the P−H group and the hydrogen positions of the amine molecules of **I**, **II**, **III**, **IV**, **V**, and **VII** compounds were initially located in the difference Fourier map, and for the final refinement, the hydrogen atoms were placed in geometrically ideal positions and refined using the riding mode. The lattice water molecules of **IV**, **VI**, and **VIII** and the amine molecules of **VI** and **VIII** were found to be disordered. The location of hydrogen positions for these molecules was not feasible, and only isotropic refinement was carried out. The extra framework atoms in **VI** were found to be highly disordered, and only a few fragments of the piperazine molecules were observed in the difference Fourier map. Hence, CHN analysis was carried out to accurately determine the formula. The last cycles of refinement included atomic positions and anisotropic thermal parameters for all of the non-hydrogen atoms. A full-matrix least-squares structure refinement against $|F|^2$ was carried out using the WINGX[17] package of programs. The poor quality of the data of **V** may be attributed to the fact that the crystal is not robust and tends to decompose during the process of data collection.

(15) *SMART*, v. 5.628; *SAINT*, v. 6.45a; *XPREP*; *SHELXTL*; Bruker AXS Inc.: Madison, WI, 2004.

(16) Sheldrick, G. M. *Siemens Area Correction Absorption Correction Program*; University of Göttingen: Göttingen, Germany, 1994.

(17) Sheldrick, G. M. *SHELXL-97*; University of Göttingen: Göttingen, Germany, 1997.

**Table 2.** Crystal Data and Structure Refinement Parameters for (a) Compounds **I**−**IV** and (b) Compounds **V**−**VIII**[a]

part a

| | I | II | III | IV |
|---|---|---|---|---|
| empirical formula | $C_{10}H_{23}N_3O_{13}PIn$ | $C_6H_6NO_5PIn$ | $C_6H_6NO_5PIn$ | $C_{12}H_{31}N_4O_{20}P_3In_2$ |
| fw | 539.10 | 317.91 | 317.91 | 873.96 |
| cryst syst | triclinic | monoclinic | monoclinic | triclinic |
| space group | $P\bar{1}$ (no. 2) | $P2(1)/c$ (no. 14) | $P2(1)/n$ (no. 14) | $P\bar{1}$ (no. 2) |
| cryst size (mm) | 0.16 × 0.12 × 0.10 | 0.16 × 0.14 × 0.08 | 0.24 × 0.12 × 0.08 | 0.20 × 0.12 × 0.08 |
| $a$ (Å) | 9.7495(16) | 8.9931(18) | 10.7198(18) | 9.195(3) |
| $b$ (Å) | 10.0012(16) | 9.2163(18) | 6.5947(11) | 12.390(4) |
| $c$ (Å) | 10.3398(17) | 11.988(2) | 13.771(2) | 13.126(4) |
| α (deg) | 93.078(3) | 90.00 | 90.00 | 76.559(5) |
| $\beta$ (deg) | 104.573(2) | 96.907(3) | 105.104(3) | 78.326(5) |
| $\gamma$ (deg) | 96.886(2) | 90.00 | 90.00 | 76.967(5) |
| vol (Å$^3$) | 965.0(3) | 986.4(3) | 939.9(3) | 1399.1(8) |
| $Z$ | 2 | 4 | 4 | 2 |
| temp (K) | 293 | 293 | 293 | 293 |
| $\rho_{calcd}$ (g cm$^{-3}$) | 1.855 | 2.141 | 2.247 | 2.074 |
| $\mu$ (mm$^{-1}$) | 1.378 | 2.553 | 2.679 | 1.912 |
| wavelength (Å) | 0.71073 | 0.71073 | 0.71073 | 0.71073 |
| $\theta$ range (deg) | 2.04−28.04 | 2.28−27.98 | 2.16−27.99 | 1.72−28.06 |
| reflns collected | 11279 | 8253 | 7835 | 15648 |
| unique reflns | 4471 | 2291 | 2210 | 6423 |
| number of params | 269 | 127 | 147 | 370 |
| goodness of fit | 1.108 | 1.052 | 1.056 | 1.094 |
| $R$ index [$I > 2\sigma(I)$] | $R_1 = 0.0315$, $wR_2 = 0.0890$ | $R_1 = 0.0402$, $wR_2 = 0.0927$ | $R_1 = 0.0316$, $wR_2 = 0.0591$ | $R_1 = 0.0349$, $wR_2 = 0.1034$ |
| $R$ (all data) | $R_1 = 0.0342$, $wR_2 = 0.0908$ | $R_1 = 0.0506$, $wR_2 = 0.0980$ | $R_1 = 0.0478$, $wR_2 = 0.0650$ | $R_1 = 0.0408$, $wR_2 = 0.1074$ |

part b

| | V | VI | VII | VIII |
|---|---|---|---|---|
| empirical formula | $C_9H_{21}N_3O_{15}P_3In_2$ | $C_8H_7N_2O_{26}P_5In_4$ | $C_4H_{10}NO_{10}SIn$ | $C_4H_0NO_{10}PIn$ |
| fw | 733.84 | 1161.29 | 379.01 | 367.84 |
| cryst syst | triclinic | triclinic | monoclinic | monoclinic |
| space group | $P\bar{1}$ (no. 2) | $P\bar{1}$ (no. 2) | $P2(1)/c$ (no. 14) | $P2(1)/c$ (no. 14) |
| crystal size (mm) | 0.16 × 0.08 × 0.06 | 0.16 × 0.10 × 0.06 | 0.24 × 0.12 × 0.08 | 0.24× 0.12 × 0.08 |
| $a$ (Å) | 6.564(3) | 8.0674(3) | 6.4779(14) | 6.4726(7) |
| $b$ (Å) | 9.346(5) | 10.0060(4) | 11.067(2) | 11.0804(11) |
| $c$ (Å) | 17.980(9) | 20.4432(9) | 14.317(3) | 14.3110(15) |
| α (deg) | 100.366(9) | 100.972(2) | 90.00 | 90.00 |
| $\beta$ (deg) | 93.170(9) | 95.0650(10) | 100.302(3) | 100.316(2) |
| $\gamma$ (deg) | 104.108(9) | 105.0530(10) | 90.00 | 90.00 |
| vol (Å$^3$) | 1046.6(9) | 1547.87(11) | 1009.9(4) | 1009.78(18) |
| $Z$ | 2 | 2 | 4 | 4 |
| temp (K) | 293 | 293 | 293 | 293 |
| $\rho_{calcd}$ (g cm$^{-3}$) | 2.329 | 2.492 | 2.493 | 2.420 |
| $\mu$ (mm$^{-1}$) | 2.514 | 3.301 | 2.597 | 2.547 |
| wavelength (Å) | 0.71073 | 0.71073 | 0.71073 | 0.71073 |
| $\theta$ range (deg) | 2.29−25.50 | 2.16−25.24 | 2.34−28.01 | 2.34−27.99 |
| reflns collected | 9214 | 21760 | 8531 | 8650 |
| unique reflns | 3459 | 5368 | 2374 | 2369 |
| number of params | 290 | 423 | 162 | 154 |
| goodness of fit | 1.127 | 1.084 | 1.122 | 1.114 |
| $R$ index [$I > 2\sigma(I)$] | $R_1 = 0.0891$, $wR_2 = 0.1735$ | $R_1 = 0.0426$, $wR_2 = 0.0989$ | $R_1 = 0.0286$, $wR_2 = 0.0687$ | $R_1 = 0.0280$, $wR_2 = 0.0795$ |
| $R$ (all data) | $R_1 = 0.1096$, $wR_2 = 0.1833$ | $R_1 = 0.0435$, $wR_2 = 0.0994$ | $R_1 = 0.0358$, $wR_2 = 0.0714$ | $R_1 = 0.0307$, $wR_2 = 0.0811$ |

[a] $R_1 = \sum||F_o| - |F_c||/\sum|F_o|$; $wR_2 = \{\sum[w(F_o^2 - F_c^2)]/\sum[w(F_o^2)^2]\}^{1/2}$. $w = 1/[\rho^2(F_o)^2 + (aP)^2 + bP]$. $P = [\max(F_o, O) + 2(F_c)^2]/3$, where $a = 0.0447$ and $b = 1.8513$ for **I**, $a = 0.0398$ and $b = 4.5394$ for **II**, $a = 0.0262$ and $b = 0.0571$ for **III**, $a = 0.0401$ and $b = 9.6472$ for **IV**, $a = 0.0000$ and $b = 57.7603$for **V**, $a = 0.0260$ and $b = 24.6108$ for **VI**, $a$ 0.0375 and $b = 0.5744$ for **VII**, and $a = 0.0420$ and $b = 2.8831$ for **VIII**.

CCDC numbers are as follows: 741941 for compound **I**, 686884 for **II**, 686885 for **III**, 741941 for **IV**, 719434 for **V**, 742100−742102 for compounds **VI**−**VIII**, and 742103 for compound **T1**. These data can be obtained free of charge from The Cambridge Crystallographic Data Center (CCDC) via www.ccdc.cam.ac.uk/data_request/cif.

## Results

**$[C_4N_2H_{12}]_3[In_2(HPO_3)_2(C_2O_4)_4]\cdot 4H_2O$, I.** The asymmetric unit of **I** contains 28 non-hydrogen atoms, of which one In and one P atom are crystallographically independent. The In atom is octahedrally coordinated by six oxygen atoms with an average In−O bond distance of 2.142 Å. Of the six In−O bonds, four belong to the oxalate bridges and two belong to the phosphite bonds. The In−O−C bond angles are in the range 113.7(2)−115.9(2)°, while those of the In−O−P bonds are in the range 112.02(16)−134.87(15)°. The P atom makes only two P−O−In bonds and possesses a terminal P═O.

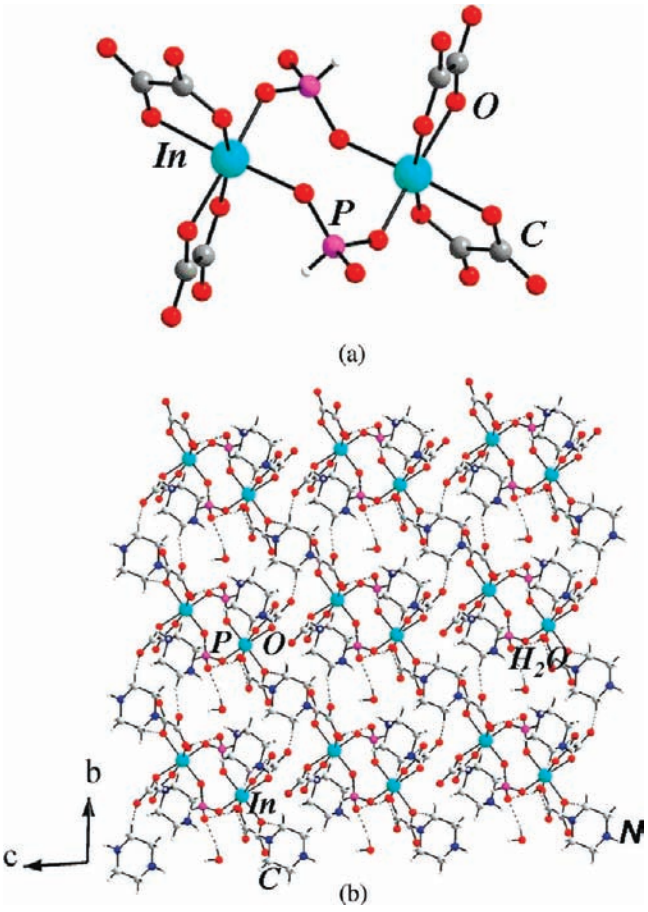


**Figure 1.** (a) Four-membered, zero-dimensional molecular structure of $[C_4N_2H_{12}]_3[In_2(HPO_3)_2(C_2O_4)_4]\cdot 4H_2O$, **I**. (b) View of the supramolecularly organized layer structure. Dotted lines represent the possible hydrogen-bond interactions.

The connectivity between the $InO_6$ and $HPO_3$ units results in the formation of a four-membered ring (Figure 1a). The oxalate moieties bind with the In center and are terminal units. This arrangement results in an anionic molecular unit of formula $[In(HPO_3)(C_2O_4)_2]^{3-}$, and the charge compensation is achieved by the presence of protonated piperazine cations. In addition to this, two lattice water molecules are present as part of the structure. The presence of anionic and cationic moieties along with water molecules in close proximity gives rise to significant hydrogen-bond interactions, leading to the formation of a supramolecularly extended structure (Figure 1b).

The molecular nature of the compound combined with the presence of water and piperazinium cations in close proximity can give rise to hydrogen-bond interactions (Table S1, Supporting Information). In **I**, we find O···O contact distances in the range of 2.720(4)−2.935(4)Å, which suggests moderate hydrogen-bond interactions. In addition, we also observed a number of C−H···O interactions, which can provide secondary support to the structure.

**$[In_2(HPO_3)_2(C_2O_4)(C_5H_5N)_2]$, II and III.** Compounds **II** and **III** have the same molecular formula with 14 non-hydrogen atoms in each of their asymmetric units, of which one In and one P atoms are crystallographically independent. The In atom in both the structures is octahedrally coordinated to five oxygen atoms and one nitrogen atom, with average In−O/N bond distances of 2.142 and 2.153 Å for **II** and **III**, respectively. Each In atom makes three In−O−P bonds and two In−O−C bonds, and the In−N bond is terminal in both of the structures. The In−O−C bond angles are in the narrow ranges of 114.0(3)−115.0(3)° and 114.7(2)−115.3°; the In−O−P bond angles are in the range 135.5(3)−149.7(4)° and 134.10(17)−146.98(19)° for **II** and **III**, respectively.

The structure of **II** consists of a network of $InO_5N$, $HPO_3$, and $C_2O_4$ units. The $InO_5N$ and the $HPO_3$ polyhedral units are connected through their vertices, forming a two-dimensional layer structure with apertures bound by four and eight T atoms (T = In and P). The oxalate units connect two different indium centers (Figure 2a and b). These oxalate units perform the dual role of completing the coordination requirement of the octahedral indium and also provide the necessary anionic charge required for charge neutrality. Since the oxalate unit is not a requirement for the formation of the two-dimensional structure in **II**, we can study the connectivity between the indium and the phosphite units. As can be seen, each nodal In or P participates in one four-ring and two eight-rings, which corresponds to the well-known structural topology described as a $4.8^2$ network (see Figure S1a of the Supporting Information). The pyridine molecule is attached to the indium metal through an In−N bond and hangs as a pendant into the interlamellar space. The layers are arranged in an AAAA... fashion (Figure 2c).

Compound **III** also consists of similar building units, the $InO_5N$, $HPO_3$, and $C_2O_4$ moieties. The $InO_5N$ and the $HPO_3$ polyhedral units are connected through their vertices to give rise to simple four-membered ring units, which are linked through their edges to form a one-dimensional ladder-like structure. The oxalate units connect two such one-dimensional ladders by binding with the indium metal, forming a two-dimensional layer with four- and eight-membered apertures (Figure 3a and b). As can be noted, the oxalate units in **III** are necessary for the formation of the two-dimensional layer structure. The pyridine molecules bind with the indium metal through In−N bonds and are positioned similar to that observed in **II**. The layers are stacked over one another in an AAAA... fashion (Figure 3c).

It is clear that both **II** and **III** are closely related and can be considered as polymorphic structures.

**$[C_4N_2H_{12}]_2[In_2(HPO_3)_3(C_2O_4)_2]\cdot 3H_2O$, IV.** The asymmetric unit of **IV** consists of 41 non-hydrogen atoms, of which two In and three P atoms are crystallographically independent. Both the indium atoms are octahedrally coordinated by six oxygen atoms, with an average In−O distance of 2.139 Å, and each indium atom makes four In−O−P bonds and two In−O−C bonds. The In−O−C bond angles are in the range 115.0(3)−116.8(3)°, while the In−O−P angles are in the range 127.96(19)−139.3(2)°. Of the three phosphorus atoms, P(1) and P(2) make three P−O−In linkages, and P(3) makes two P−O−In bonds and possesses one terminal P=O bond.

The structure of **IV** consists of a network of $InO_6$ and $HPO_3$ polyhedral units forming a two-dimensional structure. Thus, $In(1)O_6$ and $HP(1)O_3$ and $HP(2)O_3$ units are connected to each other, forming a one-dimensional corner-shared chain structure (Figure 4a). The $In(2)O_6$

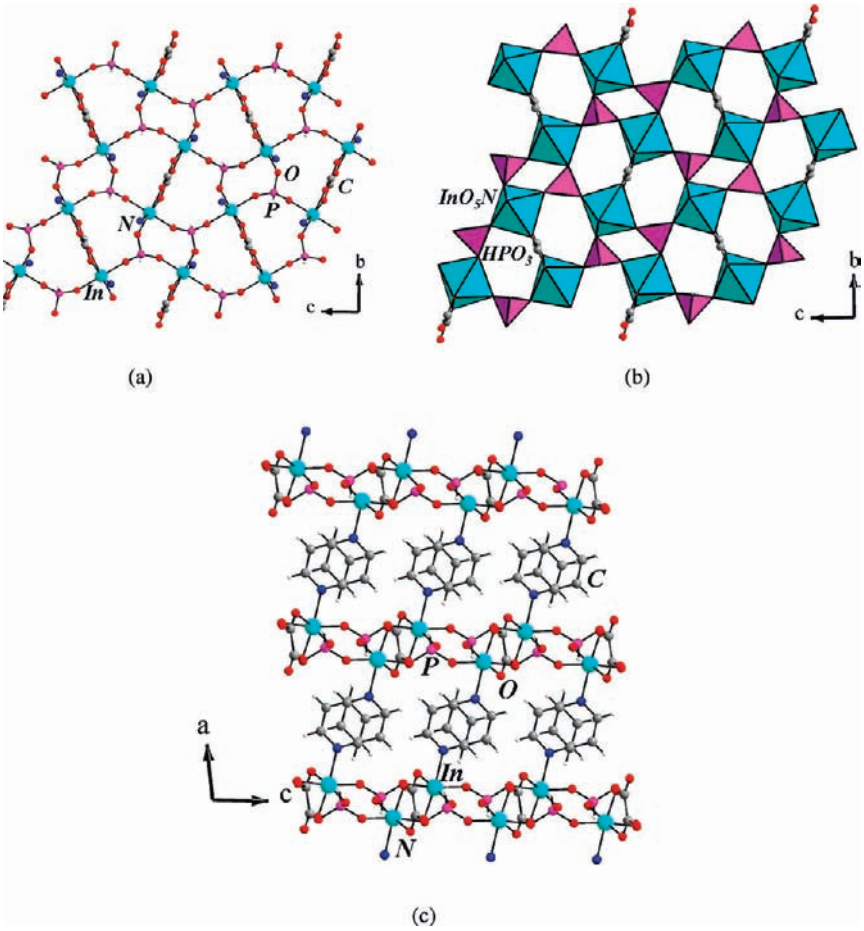


**Figure 2.** (a) View of the layer structure of $[In_2(HPO_3)_2(C_2O_4)(C_5H_5N)_2]$, **II**, along the *a* axis. Note that the oxalate units are involved only in bonding between In atoms (see text). (b) Polyhedral view of **II**. (c) Arrangement of the layers in polymorph **II**. Note the hanging pyridine molecules.

and $HP(3)O_3$ units are bound to form simple four-membered rings and connect the one-dimensional chains. This gives rise to the two-dimensional layer structure with 12-membered apertures (Figure 4b). The oxalate units are terminal and are bound to In(1) and In(2) atoms. The oxalates project on either side of the layer structure (Figure 4c). The oxalate units in **IV** also satisfy the coordination requirements of the indium atoms along with providing the necessary charge to form the macroanionic layers. The negative charge is balanced by the protonated piperazinium cations, which occupy the interlamellar space along with the water molecules.

The presence of the piperazinium cations and the water molecules in close proximity to the oxalate oxygens of the framework gives rise to a number of hydrogen-bond interactions (Table S1, Supporting Information). In **IV**, the O···O contact distances are in the range 2.764(8)−2.843(10) Å, which suggests the presence of reasonable O−H···O hydrogen-bond interactions. In addition, C−H···O hydrogen-bond interactions can also provide secondary support.

**$[C_4N_2H_{12}]_3[In_4(HPO_3)_6(C_2O_4)_3]$, V.** The asymmetric unit consists of 32 non-hydrogen atoms, of which two In and three P atoms are crystallographically independent. Each In atom is octahedrally coordinated by six oxygen atoms and makes four In−O−P and two In−O−C bonds. The In−O−C bond angles are in the range 113.2(10)−116.4(11)°, and the In−O−P bond angles are in the range 128.3(7)−140.9(8)°. The average In−O bond distance is 2.150 Å. P(1) and P(2) make three P−O−In linkages each, and P(3) makes two P−O−In bonds and possesses one terminal P═O bond.

The structure of **V** consists of a network of $InO_6$, $HPO_3$, and oxalate units forming a new type of bilayer structure. Thus, $In(1)O_6$, $In(2)O_6$, $HP(1)O_3$, and $HP(2)O_3$ units are connected to form a one-dimensional ladder-like structure. The $HP(3)O_3$ unit connects these one-dimensional ladders to form a two-dimensional layer structure with eight-membered apertures (Figure 5a). The layers are stacked over one another in an AAA... fashion, which gives rise to a layered arrangement with a supermesh of apertures. The structure possesses two types of oxalate units. While oxalate(I) connects two In(1) centers, the oxalate(II) units are terminally bonded with the In(2) centers. The oxalate(I) unit connects the In(1) centers of alternate layers, giving rise to a unique bilayer arrangement (Figure 5b). Since one of the oxalate units is terminal, this structure can be considered as an intermediate structure. The binding of the oxalates with the indium centers is in a direction perpendicular to the layers. The eight-membered apertures form a channel-like arrangement in which the piperazinium cations are located. The presence of protonated piperazine molecules in the eight-membered apertures gives rise to N−H···O- and C−H···O-type hydrogen-bond interactions (Table S1, Supporting Information). The lack of completion of

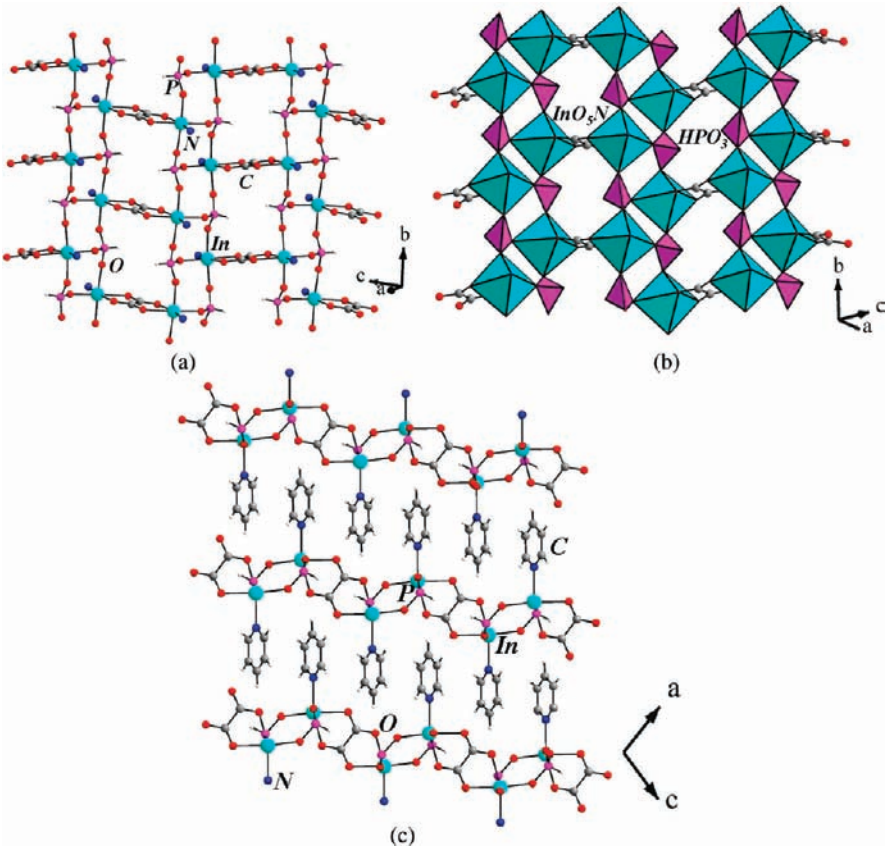


**Figure 3.** (a) View of the two-dimensional layer structure of $[In_2(HPO_3)_2(C_2O_4)(C_5H_5N)_2]$, **III**. Note the role of oxalate here (see text).(b) Polyhedral view of **III**.(c) The arrangement of layers in polymorph **III**. Note that the pyridine molecules hang in the interlamellar region.

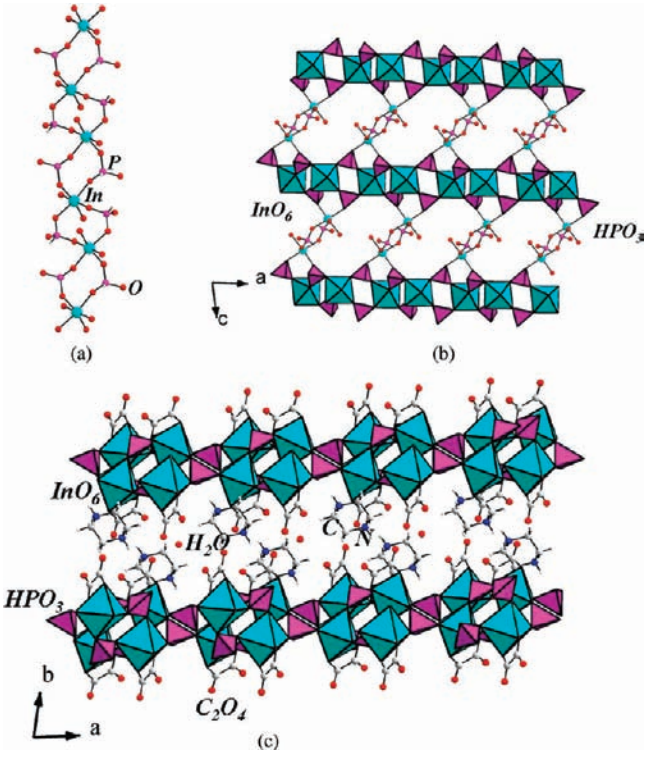


**Figure 4.** (a) View of the one-dimensional corner-shared chains in $[C_4N_2H_{12}]_2[In_2(HPO_3)_3(C_2O_4)_2]\cdot 3H_2O$, **IV**. (b) Layer structure in $[C_4N_2H_{12}]_2[In_2(HPO_3)_3(C_2O_4)_2]\cdot 3H_2O$, **IV**, with 12-membered apertures. (c) Arrangement of layers in $[C_4N_2H_{12}]_2[In_2(HPO_3)_3(C_2O_4)_2]\cdot 3H_2O$, **IV**. The amine and lattice water molecules occupy the interlayer spaces.

bonding at the In(2) centers through the oxalate makes this structure pseudo-three-dimensional in nature.

**$[C_4N_2H_{14}][In_4(H_2O)(HPO_3)_5(C_2O_4)_2]\cdot 2H_2O$, VI.** The asymmetric unit consists of 46 non-hydrogen atoms, of which four In and five P atoms are crystallographically independent. Each In atom is octahedrally coordinated by six oxygen atoms. While In(1), In(2), and In(3) make two In−O−C and four In−O−P bonds, In(4) has two In−O−C and three In−O−P bonds and possesses one In−$H_2O$ terminal bond. The In−O−C bond angles are in the range 114.0(5)−125.1(6)°, while those of the In−O−P bonds are in the range 130.7(4)−155.7(4)°. The average In−O bond distance is 2.138 Å. All of the P atoms make three P−O−In bonds each.

The structure of **VI** also has similar building units to those observed in the other members of this family of compounds. The present structure is different in that it has three-dimensional connectivity arising out of the bonding between the $InO_6$, $HPO_3$, and the oxalate units. $InO_6$ and $HPO_3$ units are connected to form a two-dimensional layer that is very different from the layers observed in any other indium phosphite structures reported in the literature.[18] The layer structure can be considered as being formed by the linkage between two ladder structures, except that the ladders are interrupted, resulting in short ladder arrangements (Figure 6a). The interruption in the arrangement is due to the lack of the

(18) (a) Yi, Z.; Chen, C.; Li, S.; Li, G.; Meng, H.; Cui, Y.; Yang, Y.; Pang, W. *Inorg. Chem. Commun.* **2005**, *8*, 166. (b) Wang, L.; Song, T.; Xu, J.; Wang, Y.; Tian, Z.; Shi, S. *Microporous Mesoporous Mater.* **2006**, *96*, 287.

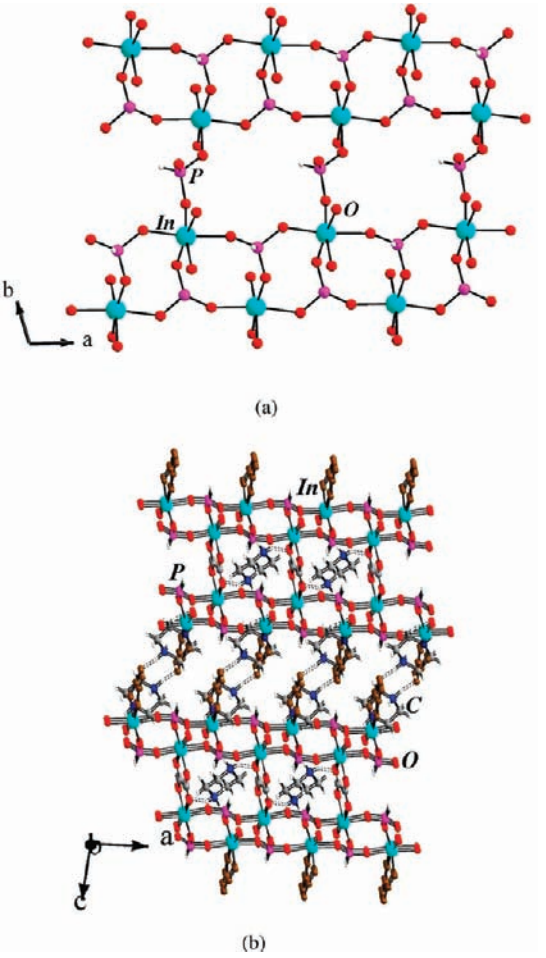


**Figure 5.** (a) View of the layer structure in $[C_4N_2H_{12}]_3[In_4(HPO_3)_6(C_2O_4)_3]$, **V**, in the *ab* plane. (b) View of the "double-layer" structure of $[C_4N_2H_{12}]_3[In_4(HPO_3)_6(C_2O_4)_3]$, **V**. The terminal oxalate units are shown in brown. Dotted lines represent the possible hydrogen-bond interactions. Note the dual role of the oxalate units.

phosphorus atom, which appears to have shifted its position to act as a cap on the four-membered ring of the ladder, giving rise to a SBU-5 building unit.[2] This shifting can also be visualized schematically (see the Supporting Information, Figure S2). This type of connectivity is new and results in 4-, 8-, and 16-membered apertures within the layer. The structure also possesses two types of oxalate units, *in-plane* and *out-of-plane*. The in-plane oxalate units occupy the middle of the 16-membered apertures within the indium phosphite layer by binding with In(1) and In(2) centers (Figure 6b). The oxalate units reduce the size of the 16-membered apertures to eight-membered ones, as such large apertures in hybrid compounds are rarely observed. The other oxalate units (out of-plane) link two such layers to give rise to the three-dimensional structure (Figure 7). This arrangement gives rise to two distinct types of eight-membered channels, wherein the disordered 1,4-diaminobutane molecules are located.

**$[C_4N_2H_{12}][In_2(H_2O)_2(SO_4)_2(C_2O_4)_2]\cdot 2H_2O$ and $[C_4N_2H_{12}][In_2(H_2O)_2(HPO_4)_2(C_2O_4)_2]\cdot 2H_2O$, VII and VIII.** The sulfate−oxalate and phosphate−oxalate compounds of indium are isostructural. The asymmetric units consist of 17 non-hydrogen atoms, of which one In and one M (M = S, P) are crystallographically independent.

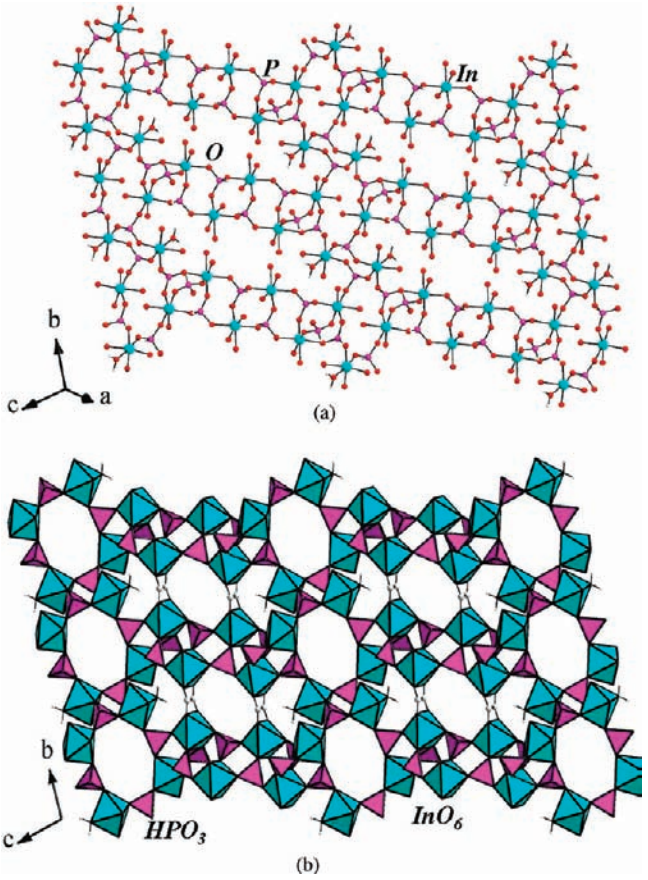


**Figure 6.** (a) View of the layers in $[C_4N_2H_{14}][In_4(H_2O)(HPO_3)_5(C_2O_4)_2]$, **VI**. (b) Polyhedral view of the layers of **VI** in the *bc* plane. Note that the oxalate units bridge the In atoms within the layer (see text).

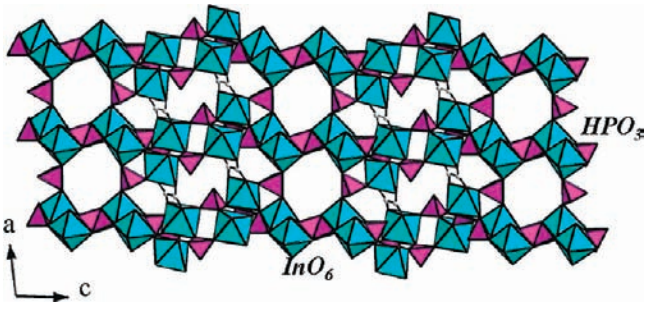


**Figure 7.** Polyhedral view of the three-dimensional structure of $[C_4N_2H_{14}][In_4(H_2O)(HPO_3)_5(C_2O_4)_2]$, **VI**. The oxalate units have *in-plane* and *out-of-plane* connectivity in this structure.

The In atoms are coordinated by seven oxygen atoms and have a distorted pentagonal bipyramidal geometry (Figure 8a). The In−O−C bond angles are in the range 115.7(2)−117.6(2)°, while those of the In−O−M bonds are in the range 129.6(2)−130.1(2)°. The average In−O bond distances are 2.212 and 2.221 Å for **VII** and **VIII**, respectively. In both of the compounds, the M (S, P) atom makes two M−O−In bonds and possesses two terminal M−O bonds. In the case of the phosphorus-containing compound, we observed a proton position near one of the oxygens [O(9)], making it a P−OH group.

The compounds **VII** and **VIII** have similar structures. The $InO_7$ pentagonal bipyramidal units and $SO_4/HPO_4$ tetrahedra are connected through their vertices to form

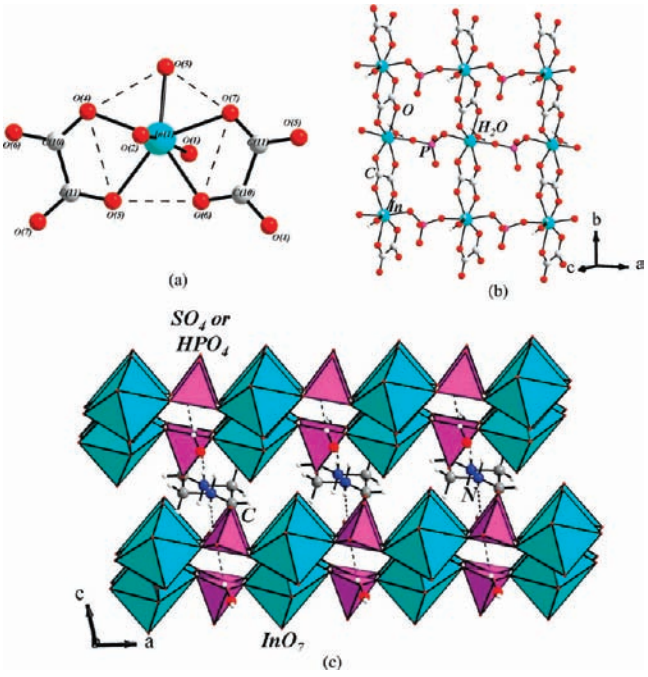


**Figure 8.** (a) Coordination around In in $[C_4N_2H_{12}]_{0.5}[In(H_2O)(MO_4)(C_2O_4)]\cdot H_2O$, M(S, HP) in **VII** and **VIII**. Note the pentagonal bipyramidal arrangement. (b) Layer structure observed in compounds **VII** and **VIII**. Note that the oxalate units connect two wire-like one-dimensional structures. (c) Polyhedral view of the layer observed in **VII** and **VIII** along the *b* axis. Note the presence of amine molecules in the interlamellar space. Dotted lines represent possible hydrogen-bond interactions.

one-dimensional wire-like units along the *a* axis (Figure 8b). These indium phosphate/sulfate units are cross-linked by the oxalate units to give rise to a macroanionic layered structure with eight-membered apertures. Charge compensation is achieved by the presence of the protonated piperazinium cations, which are located in the interlamellar spaces along with the lattice water molecules. In addition to this, a water molecule is also bound to the In atom. We observed N−H···O, C−H···O, and O−H···O hydrogen-bond interactions in **VII** (Table S1, Supporting Information, and Figure 8c). The amine molecules were found to be disordered in compound **VIII**.

## Discussion

**Synthesis.** The compounds **I**−**VIII** are members of a family of inorganic−organic hybrid framework structures and were obtained as good-quality single crystals by hydrothermal methods (Table 1). All of the materials involve connectivity between the indium, the phosphite/phosphate/sulfate moieties, and the oxalate units. Compound **I** has a zero-dimensional structure; **II**, **III**, **IV**, **VII**, and **VIII** have two-dimensional structures; compound **V** has a unique bilayer structure; and **VI** has a three-dimensional structure. All of the compounds were prepared employing organic amines as the structure-directing agent.

Of the eight compounds synthesized in the present study, the zero-dimensional structure of **I** is important. To the best of our knowledge, this is the first molecular inorganic−organic hybrid open-framework structure. Compounds **II** and **III** have pyridine molecules acting as ligands by binding with the indium centers and are polymorphic in nature. Compound **VII** was obtained serendipitously during our synthetic attempts. Acting on a clue, we explored the preparation of the phosphate phase, **VIII**, using modified synthetic conditions (Table 1).

From the synthesis conditions, it appears that the hybrid structures form over a wide range of pH's. The three-dimensional phase forms at acidic pH and lower temperatures. Similar observations have been made previously during the preparation of phosphite−oxalate structures of iron.[13a] The formation of **II** and **III** with bound pyridine molecules suggests that the indium center may be amenable to attack by the organic bases at near-neutral pH values. Though the reaction mixture contains 1,4-diaminobutane (1,4-DAB), it was not incorporated in the final product, suggesting a secondary role for 1,4-DAB in the preparations. The presence of 1,4-DAB is necessary for isolating **III** as a minor phase, and in its absence the reaction mixture gives rise to compound **II** as a pure phase.

Compounds **II** and **III** have been obtained from the same reaction mixture and have comparable structures. Hence, they can be considered as concomitant polymorphs. The isolation of concomitant polymorphic structures in the present study indicates competing reactions under hydrothermal conditions. It has been observed that multiple but unrelated phases are formed during hydrothermal reactions.[6b,19]

It is to be noted that compounds **II** and **III** were prepared in the presence of HF in the reaction mixture but did not get incorporated in the framework. The fluoride ion has been used as a mineralizer in the synthesis of many silicate and phosphate framework structures.[20] The formation of cloverite, employing HF in the synthesis, however, led to the incorporation of fluorine as part of the framework.[21] This observation, indeed, opened up the use of HF in the preparation of open-framework structures. It has been generally believed that the framework building units can be altered by the use of HF.[20] Thus, oxofluorometal species involving the main group elements formed in solution can interact with the organic amine molecules through weak hydrogen-bond interactions, giving rise to new structures and compositions.[20] In the present case, during the synthesis of **II** and **III**, we believe that the HF essentially acts as a mineralizer by creating suitable building units. This role of HF has been extensively documented in the literature.[22] We observed that the absence of HF, however, leads to the formation of unidentified amorphous phases. HF, thus, appears to be necessary for the stabilization of **II** and **III** by acting as a mineralizer.

The zero-dimensional compound, **I**, and the double-layer compound, **V**, have been prepared employing the

(19) (a) Rao, V. K.; Chakrabarti, S.; Natarajan, S. *Inorg. Chem.* **2007**, *46*, 10781. (b) Gandara, F.; O'Shea, F.; de la P., V. A.; Illas, F.; Snejko, N.; Proserpio, D. M.; Puebla, E. G.; Monge, M. A. *Inorg. Chem.* **2009**, *48*, 4707.
(20) (a) Weigel, S. J.; Gabriel, J. C.; Puebla, E. G.; Bravo, M. A.; Henson, N. J.; Bull, L. M.; Cheetham, A. K. *J. Am. Chem. Soc.* **1996**, *118*, 2427. (b) Morris, R. E.; Weigel, S. J. *Chem. Soc. Rev.* **1997**, *26*, 309.
(21) Esterman, M.; McCusker, L. B.; Baerlocher, C.; Merrouche, A.; Kessler, H. *Nature* **1991**, *352*, 320.
(22) Chang, W.-J.; Chang, P.-C.; Kao, H.-M.; Lii, K.-H. *J. Solid State Chem.* **2005**, *178*, 3709. (b) Serpaggi, F.; Loiseau, T.; Ferey, G. *Acta Crystallogr.* **1997**, *c53*, 1568. (c) Chen, C.; Yi, Z.; Ding, H.; Li, G.; Bi, M.; Yang, Y.; Li, S.; Li, W.; Pang, W. *Microporous Mesoporous Mater.* **2005**, *83*, 301.

same synthesis mixture but at different temperatures. This observation suggests that compound **I**, which is molecular, could be the precursor for the formation of the more stable **V**.

**Structure.** During the present study, we have prepared a series of hybrid structures of indium of varying dimensionality. Of these, the isolation of the molecular structure, **I**, is important. The molecular structure comprises of a simple four-membered ring made up of In and P with the oxalate units being terminal. A careful analysis of all of the structures reveals that the four-membered ring is the smallest SBU. The connectivity between the four-membered rings is different among the structures. Thus, the four-membered rings are connected edgewise to form a ladder in one of the polymorphs (**III**) and also in compound **V**. The four-membered rings are connected through the corners in **IV** and are interrupted in **VI**. These observations clearly suggest that the four-membered ring plays a crucial role in the formation of the structures described in the present study.

The structure of **II** can be compared with the indium phosphite−oxalate compound, $[C_6H_{14}N_2][In_2(HPO_3)_3(C_2O_4)]$, reported in the literature.[23] Both of the structures have comparable layer arrangements, but the $[C_6H_{14}N_2][In_2(HPO_3)_3(C_2O_4)]$ has a three-dimensional structure (Figure S11, Supporting Information). In **II**, the terminal pyridine molecules, bound to the indium atoms, restrict the extension of the structure in the third dimension.

The role of oxalates in the formation of hybrid structures has been discussed before.[13a] The formation of the *in-plane* and the *out-of-plane* connectivities of the oxalates appears to modify the structure and extend the dimensionality. This, in a way, is similar to the use of 4,4′-bipyridine in some of the framework hybrid structures.[24] The oxalates, on the other hand, possess negative charge (anionic), and hence their role is significant. We find terminal oxalate units in some of the present structures (**I**, **IV**, and **V**), which has not been observed before in many of the hybrid structures. Recently, terminal oxalate structures have been observed in $(H_3DETA)[Fe_3(C_2O_4)_2(HPO_4)_2(PO_4)]$[11] and $[NH_3CH_2CH_2NH_3]_{2.5}[Al_4H(HPO_4)_4(H_2PO_4)_2(C_2O_4)_4]$.[14a] The presence of oxalate units satisfying only the coordination or charge requirements (in structures **II** and **VI**) has not been observed frequently. This type of bonding of the oxalate units has been observed previously in $[C_8N_4H_{26}][Fe^{III}{}_6(HPO_3)_8(C_2O_4)_3]\cdot 4H_2O$.[13a] The variable nature of the connectivity of the oxalate units is also seen in the structure of **VI**, wherein the oxalate performs a dual role. The observation of the different roles for the oxalate units in the polymorphic structures of **II** and **III** suggests that the oxalate bonding is highly flexible. Understanding the nature of oxalate bonding in hybrid frameworks would help in obtaining better control over the design of new networks.

**Polymorphism in Structures II and III.** Polymorphism and intergrowth phases are common among the aluminosilicate zeolites.[25] Polymorphic phases in amine templated structures, on the other hand, are quite rare. In open-framework compounds, polymorphic structures have been observed in zinc phosphite,[6b] zinc arsenate,[19a] and other related compounds.[19b,26] During the present study, we have prepared two polymorphic phases, **II** and **III**, from the same reaction mixture concomitantly.

The compounds have the same molecular formula but crystallize in two different space groups. Compounds **II** and **III** also exhibit visible morphological differences (insets a and b, Figure 9). From the synthesis point of view, polymorph **III** is a minor phase compared to polymorph **II**. In spite of our repeated attempts, we have been able to neither improve the yield nor prepare a pure phase of **III**, which precluded its satisfactory characterization. Since we formed **II** as the major phase in all of our preparations, and have also been successful in preparing it as a single phasic solid by modifying the synthesis conditions, it is clear that this polymorph is more stable compared to the other. In order to understand this, we have performed preliminary DFT calculations on the structures of the polymorphs to probe the relative stabilities of **II** and **III**.

The large unit cell size along with the number of atoms makes the periodic calculations difficult. In addition, converging the energy with respect to a tight energy cutoff also becomes practically unattainable. A more convenient and chemically insightful calculation can be performed by considering a small cluster of dimensions $30 \times 30 \times 30$ Å$^3$, along with maintaining the coordination spheres of In, P, and C atoms of the original structure. Hydrogen atoms were added at the "cutoff" points to passivate the dangling bonds, and the positions of such hydrogen atoms were optimized while keeping the rest of the atoms fixed. All of the calculations were performed using the Amsterdam Density Functional package[27−29] employing the Perdew−Burke−Ernzerhof exchange-correlation functional[30] at the double-$\zeta$ basis set level.[31] The optimized structures for the clusters are shown in Figure 9a and b. The calculated binding energies for **I** and **II** were found to be −2.73 eV/bond and −1.85 eV/bond, respectively. This shows that **II** is stabilized by 0.88 eV/bond with respect to the other cluster, **III**, and suggests that the formation of **II** may be favored over **III**, which is also consistent with the experimental observations.

**Transformation Reactions.** It has been established that the low-dimensional structures could be the precursors for structures of higher dimensionality under appropriate conditions.[32] In the present study, we had the fortuitous

(23) Li, H.; Zhang, L.; Liu, L.; Jiang, T.; Yu, Y.; Li, G.; Huo, Q.; Liu, Y. *Inorg. Chem. Commun.* **2009**, *12*, 1020.
(24) (a) Chang, W.-J.; Jiang, Y.-C.; Wang, S.-L.; Lii, K.-H. *Inorg. Chem.* **2006**, *45*, 6586. (b) Huang, L.-H.; Kao, H.- M.; Lii, K.-H. *Inorg. Chem.* **2002**, *41*, 2936. (c) Hung, L.-I.; Wang, S.-L.; Kao, H.-M.; Lii, K.-H. *Inorg. Chem.* **2002**, *41*, 3929. (d) Chang, W.-K.; Chiang, R.-K.; Jiang, Y.-C.; Wang, S.-L.; Lee, S.-F.; Lii, K.-H. *Inorg. Chem.* **2004**, *43*, 2564.
(25) Rao, C. N. R.; Thomas, J. M. *Acc. Chem. Res.* **1985**, *18*, 113.
(26) (a) Wiebcke, M.; Marler, B. *Solid State Sci.* **2004**, *6*, 213. (b) Natarajan, S.; Prots, Y.; Ewald, B.; Niewa, R.; Kniep, R. *Z. Anorg. Allg. Chem.* **2006**, *632*, 37. (c) Herschke, L.; Enkelmann, V.; Lieberwirth, I.; Wegner, G. *Chem.—Eur. J.* **2004**, *10*, 2795.
(27) te Velde, G.; Bickelhaupt, F. M.; van Gisbergen, S. J. A.; Fonseca Guerra, C.; Baerends, E. J.; Snijders, J. G.; Ziegler, T. *J. Comput. Chem.* **2001**, *22*, 931.
(28) Fonseca Guerra, C.; Snijders, J. G.; te Velde, G.; Baerends, E. J. *Theor. Chem. Acc.* **1998**, *99*, 391.
(29) *ADF2007.01*; SCM, Theoretical Chemistry, Vrije Universiteit: Amsterdam, The Netherlands. http://www.scm.com (accessed Nov 2009).
(30) Perdew, J. P.; Burke, K.; Ernzerhof, M. *Phys. Rev. Lett.* **2006**, *77*, 3865.
(31) Davidson, E.; Feller, D. *Chem. Rev.* **1986**, *86*, 681.
(32) (a) Ayi, A. A.; Choudhury, A.; Natarajan, S.; Neeraj, S.; Rao, C. N. R. *J. Mater. Chem.* **2001**, *11*, 1181. (b) Rao, C. N. R.; Natarajan, S.; Choudhury, A.; Neeraj, S.; Ayi, A. A. *Acc. Chem. Res.* **2001**, *34*, 80.

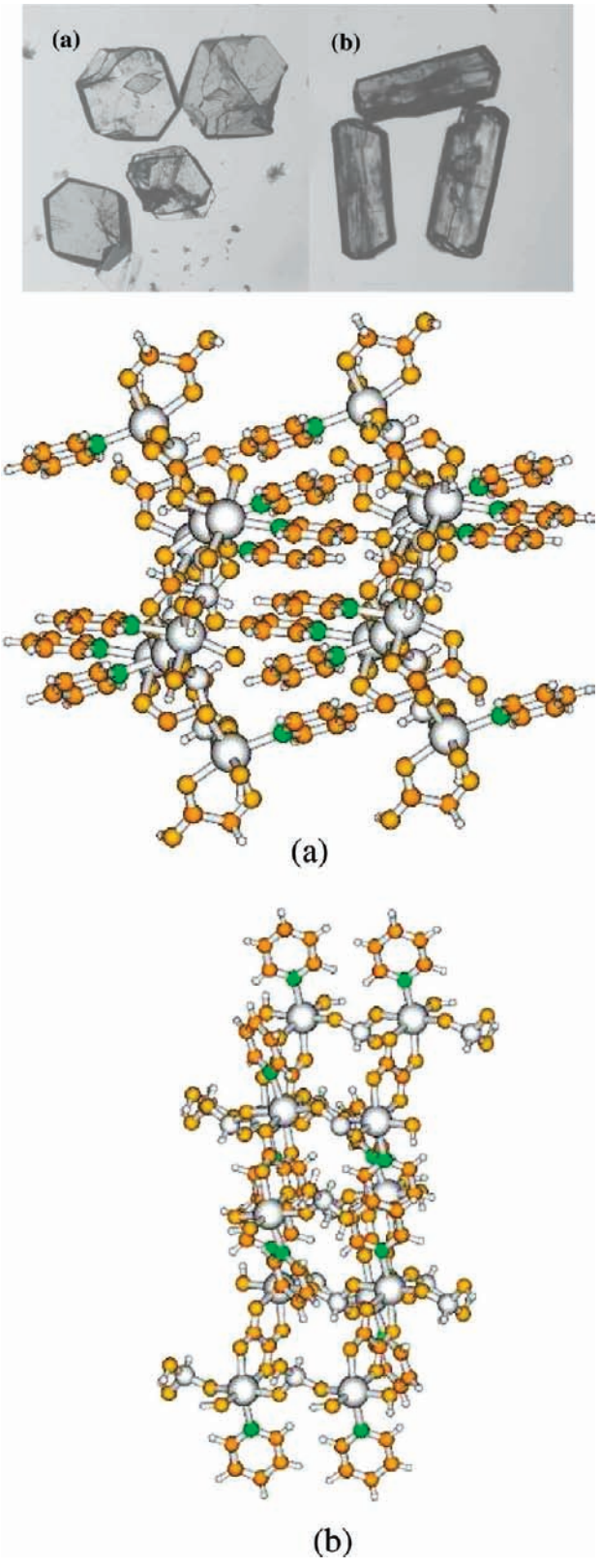


**Figure 9.** View of the density functional theory optimized structures of (a) polymorph **II** and (b) polymorph **III**. Inset shows the optical photograph of the crystals of the two polymorphic phases.

coincidence of isolating the first zero-dimensional hybrid structure, $[C_4N_2H_{12}]_3[In_2(HPO_3)_2(C_2O_4)_4]\cdot 4H_2O$, **I**, which prompted us to investigate the reactivity of this structure. Recently, we have shown that molecular zinc arsenates are reactive and transform under suitable conditions to structures of higher dimensionality.[19a] The transformation studies on molecular amine templated compounds clearly established the stabilization of higher dimensional structures that are not easily prepared by the usual routes (reacting the individual components).[32] Since we have not been able to synthesize polymorph **III** as a pure phase, we wanted to investigate the formation of **III** from the molecular compound **I** under suitable conditions. Thus, compound **I** (0.125 g) was taken in a 23 mL PTFE-lined autoclave and heated in the presence of pyridine (1.3 mL), 1,4-diaminobutane (0.1 mL), and water (1 mL) at 180 °C for 48 h. A similar reaction was also carried out in the absence of 1,4-diaminobutane as well. The initial pH of the reaction mixtures was ~7.5, and the final pH was ~5.0. In both of these reactions, the product phase was found to be the single phase of **II**. The transformation reactions suggest that **I** is reactive. To further clarify whether the transformation reaction goes through any intermediate phases, we have carried out time-dependent studies. For this, several autoclaves with the same reaction compositions were taken and heated in the same oven for varying periods of time. In all of the cases, the product phase was isolated, washed, dried under ambient conditions, and investigated using powder XRD.

The time-dependent studies (Figure 10) indicate the formation of an unidentified phase (∗) during the course of the transformation reactions, along with the formation of compound **III** after 6 h. Upon prolonged heating, the XRD patterns did not reveal any additional changes up to 24 h. Upon heating further, the formation of polymorph **II** was observed, along with polymorph **III** and the unidentified phase. The unidentified phase (∗) completely vanishes after 36 h. Further heating leads to the loss of **III** in the product phase (after 42 h) and results in the formation of a single phase of **II**. This observation suggests that the transformation pathway of molecular compound **I** goes through a reactive intermediate. It has been postulated previously that molecular compounds could transform via one-dimensional intermediates that have either a ladder or a chain structure.[32a,33] It is highly likely that, in the present study also, molecular compound **I** undergoes transformation via a similar pathway. Since the intermediate has not been identified structurally, we can suggest the structure of the intermediate as a possible one-dimensional hybrid structure (see the Supporting Information, Figure S3). Interestingly, it may be noted that the less stable polymorph **III** was observed before the formation of **II**. This observation suggests that polymorph **III** could be a transient phase which transforms to **II**; this would also explain the much lower yield during the regular synthesis.

**Transformation of Compound I to the Three-Dimensional Indium Phosphite, $[C_4N_2H_{12}][In_4(H_2O)_3(HPO_3)_7]$, T1.** Similar to the transformation studies in the presence of pyridine, we wanted to explore the reactivity of the molecular compound, **I**, in the presence of phosphorous acid as a function of time at 180 °C. For this, compound **I** (0.125 g) was taken in a 23 mL PTFE-lined autoclave and

(33) Dan, M.; Udayakumar, D.; Rao, C. N. R. *Chem. Commun.* **2003**, *17*, 2212.

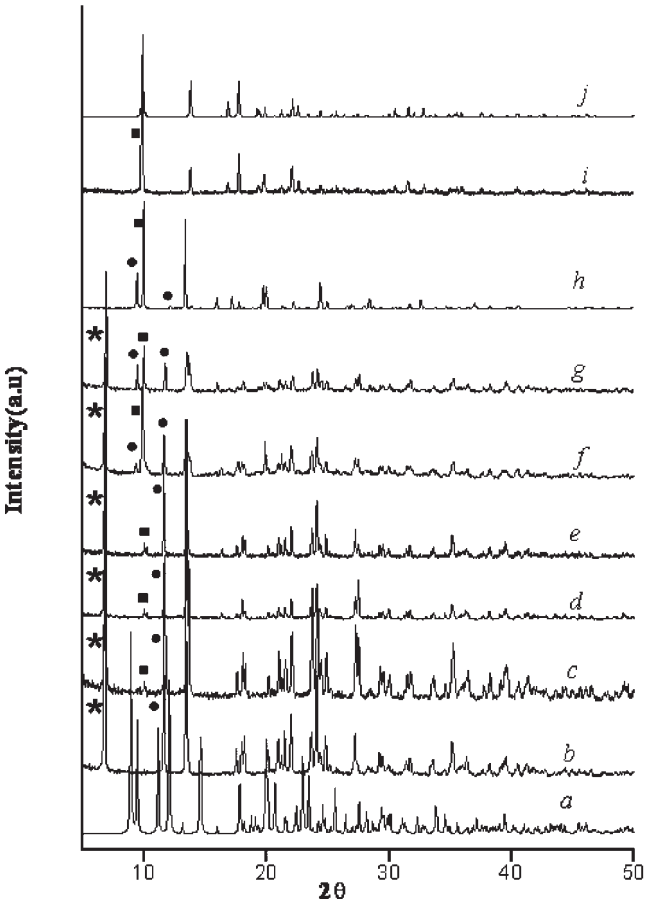


**Figure 10.** Time-dependent powder X-ray diffraction patterns of the product of the transformation reaction of the zero-dimensional molecular compound $[C_4N_2H_{12}]_3[In_2(HPO_3)_2(C_2O_4)_4]\cdot 4H_2O$, **I**. (a) Simulated pattern of **I**. Experimental pattern of **I** + py (b) after 6 h, (c) after 12 h, (d) after 18 h, (e) after 24 h, (f) after 30 h, (g) after 36 h, (h) after 42 h, and (i) after 48 h. (j) Simulated pattern of compound **II** (● denotes XRD lines due to polymorph **III**; ■ denotes the first XRD line of polymorph **II**; ∗ denotes unidentified phase). Note that polymorph **III** is formed before polymorph **II** (see text).

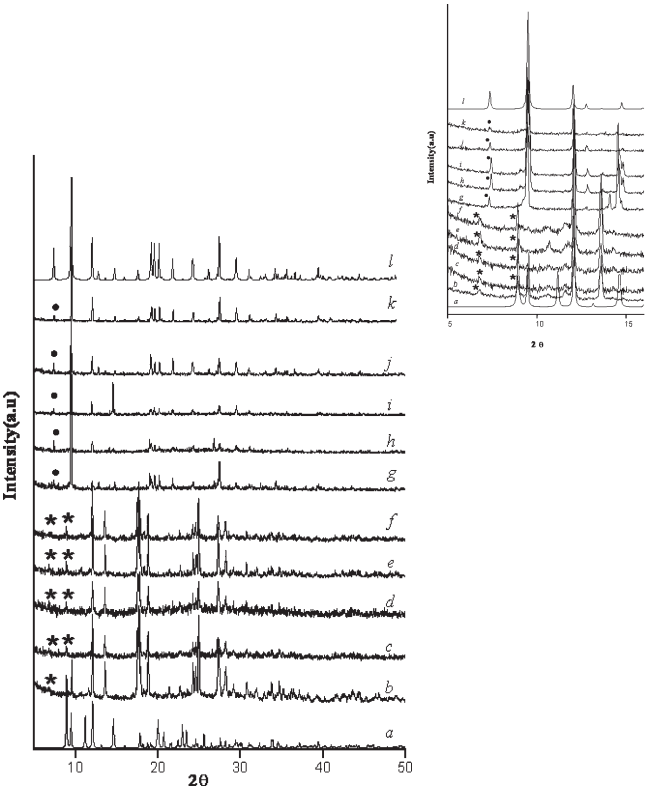


**Figure 11.** Time-dependent powder X-ray diffraction patterns of the product of the transformation reaction of the zero-dimensional molecular compound $[C_4N_2H_{12}]_3[In_2(HPO_3)_2(C_2O_4)_4]\cdot 4H_2O$, **I**, to the three-dimensional indium phosphite $[C_4N_2H_{12}][In_4(H_2O)_3(HPO_3)_7]$, **T1**. (a) Simulated pattern of **I**. Experimental pattern of **I** + phosphorous acid (b) after 1 h, (c) after 3 h, (d) after 5 h, after 6 h, (f) after 12 h, (g) after 18 h, (h) after 24 h, (i) after 36 h, and (k) after 48 h. (l) Simulated pattern of compound **T1**. (∗ denotes unidentified phase; ● denotes XRD lines of the compound **T1**). Inset shows the X-ray powder patterns from $2\theta$ 5−16°.

heated in the presence of phosphorous acid (0.084 g) and water (2 mL) at 180 °C for 48 h. The initial pH of the reaction mixture was 2.0, and there was no appreciable change in pH during the course of the reaction. The resulting product was found to contain good-quality hexagonal-shaped single crystals and was found to correspond to the three-dimensional indium phosphite, $[C_4N_2H_{12}][In_4(H_2O)_3(HPO_3)_7]$, **T1**.

To further investigate the possible pathway for the transformation reaction, a time-dependent study was carried out at 180 °C (Figure 11 and Figure S4, Supporting Information). The XRD patterns of the product phases show that, upon heating the molecular compound with phosphorous acid, an unidentified intermediate phase (∗) is formed, which lasts for ∼12 h. Upon further heating, the phase **T1** forms as a pure phase after 36 h. It is to be noted that, though the oxalate anion was present in the initial zero-dimensional compound **I**, the final three-dimensional phase **T1** forms without the oxalate. This suggests that the transformation reaction could proceed via a dissolution and recrystallization route. A similar observation, involving the transformation of a one-dimensional iron arsenate−oxalate $[C_4N_2H_{12}][Fe(OH)(HAsO_4)(C_2O_4)]\cdot H_2O$ to a three-dimensional iron arsenate $[C_4N_2H_{12}][Fe_2^{III}Fe_1^{II}(AsO_4)_2(HAsO_4)_2]$, has been reported previously.[12a]

Since a new indium phosphite phase was observed, we have carried out a single crystal structural study of the compound. The structural description is given below.

The asymmetric unit of the compound **T1** contains 16 non-hydrogen atoms, of which three In and three P atoms are crystallographically independent. Of these, two In atoms, In(1) (at 2b) and In(2) (at 2a), and one phosphorus atom, P(3) (at 4d), occupy special positions, with site multiplicities of 0.16 for In(1) and In(2) and 0.33 for P(3). Each In atom is octahedrally coordinated by six oxygen atoms with an average In−O bond distance of 2.135 Å. The O−In−O bond angles are in the range 82.9(3)−180.0(8)°. While In(1) and In(2) make six In−O−P bonds each, In(3) makes five In−O−P bonds and possesses one terminal In−$H_2O$ bond. The In−O−P bond angles are in the range 131.7(5)−148.7(6)°. The average P−O bond distance is 1.518 Å, and the average O−P−O bond angle is 112.34°. Selected bond angles and distances for compound **T1** are provided in Table S4 (Supporting Information). The extra framework atoms were found to be highly disordered, and only a few fragments of the piperazine molecules were observed in the difference Fourier map. Hence, CHN analysis was carried out to accurately determine the formula (see the Supporting

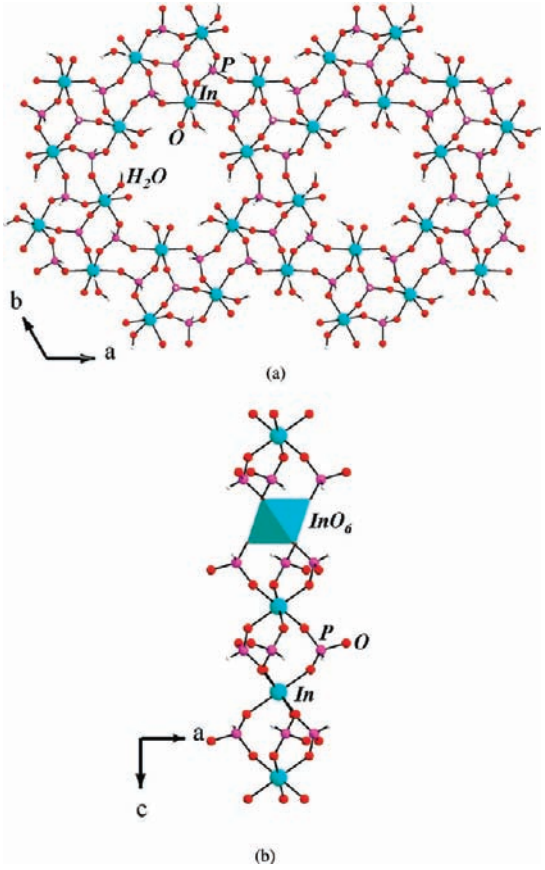


**Figure 12.** (a) View of the indium phosphite layers, $[In_3(H_2O)_3(HPO_3)_4]^+$, in **T1**. (b) One-dimensional chain structure, $[In(HPO_3)_3]^{3-}$, that connects the layers in **T1**.

Information). Pertinent experimental details of the structure determination are presented in Table S5 of the Supporting Information.

The structure of **T1** consists of a network of $InO_6$, $InO_5(H_2O)$, and $HPO_3$ units connected through their vertices to form a layer of the formula $[In_3(H_2O)_3(HPO_3)_4]^+$, encompassing circular 12-membered rings as shown in Figure 12a. This layer arrangement has been observed in many aluminophosphates based on the $[Al_3(PO_4)_4]^{3-}$ macroanion.[34] The 12-membered rings are surrounded by a series of four-membered rings. In one set of rings, the phosphorus atoms form a part of the wall of the 12-membered apertures, while in the other set, a $HP(3)O_3$ group caps a six-membered ring and alternates above and below the plane of the12-membered aperture. These layers, which can be described as 4.6.12 nets,[35] are arranged in an AAA... fashion.

The 12-membered apertures in **T1** are filled with one-dimensional chain/wire structures that propagate in a direction that is perpendicular to the layer arrangement. The one-dimensional chain units are formed by the connectivity between $In(1)O_6$, $In(2)O_6$, and $HP(1)O_3$ polyhedra (Figure 12b). Thus, the $In(1)O_6$ and $HP(1)O_3$ units fill the 12-membered apertures (Figure S5a, Supporting Information) and are connected to the next nearest neighbor layer via $In(2)O_6$ polyhedra. This arrangement, thus, resembles a pillared layer structure (Figure 13). Similar pillared structures have recently been observed in an indium phosphate $[C_{10}N_2H_9]_3[In_9(HPO_4)_{14}(H2O)_6F_3]\cdot(H_3O)\cdot(H_2O)_2$;[36a] in an iron phosphite, $[C_4N_2H_{12}][Fe_4(H_2O)_3(HPO_3)_7]\cdot(H_2O)_x$ ($x = 0.6$);[36b] and in an iron arsenate, $[4,4'\text{-bpyH}_2]_3[Fe_9(H_2O)_6F_3(HAsO_4)_{12}(AsO_4)_2]\cdot 2H_2O$.[36c]

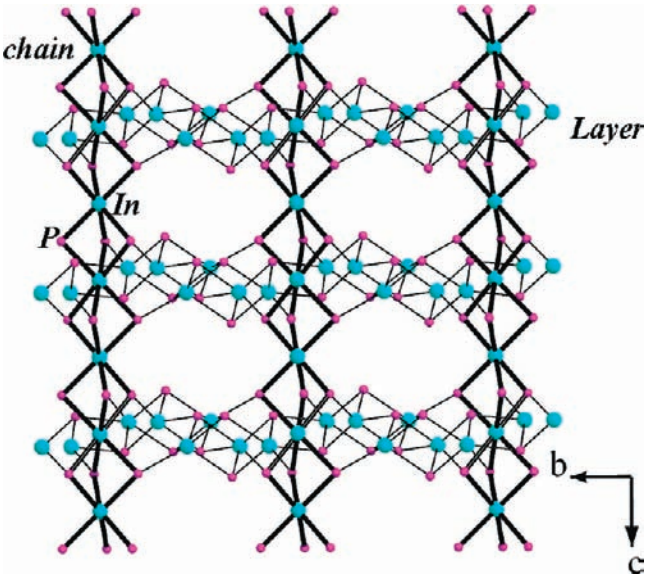


**Figure 13.** View of the T-atom (T = In, P) connectivity showing the three-dimensional structure of $[C_4N_2H_{12}][In_4(H_2O)_3(HPO_3)_7]$, **T1**. The disordered amine molecules are not shown.

The present transformation studies indicate that the molecular hybrid compound **I** is reactive and could be employed as a precursor for the formation of higher dimensional structures. To probe and investigate further, one needs to employ in situ experiments in the presence of powerful sources of radiation such as the synchrotron. Such studies have been undertaken before,[37] which shed light on the intermediate phases, kinetics, and other related phenomena that are important in the crystallization process during hydrothermal synthesis.

**The Proton-Decoupled $^{31}$P CPMAS NMR Spectroscopic Studies.** The proton-decoupled $^{31}$P CPMAS NMR spectroscopic studies have been carried out on a Bruker-AVIII 500 spectrometer operating at 11.7 T with resonance frequencies of 202.47 MHz for $^{31}$P. $H_3PO_4$ (85%) was used as the external standard, and the chemical shifts are relative to the phosphoric acid. The observed $^{31}$P spectra and the number of chemical shifts observed are in agreement with the single-crystal study for the

(34) (a) Thomas, J. M.; Jones, R. H.; Xu, R.; Chen, J.; Chippindale, A. M.; Natarajan, S.; Cheetham, A. K. *J. Chem. Soc., Chem. Commun.* **1992**, 929. (b) Barrett, P. A.; Jones, R. H. *J. Chem. Soc., Chem. Commun.* **1995**, 1979. (c) Oliver, S.; Kuperman, A.; Lough, A.; Ozin, G. A. *Inorg. Chem.* **1996**, *35*, 6373. (d) Chippindale, A. M.; Cowley, A. R.; Huo, Q.; Jones, R. H.; Law, A. D.; Thomas, J. M.; Xu, R. *J. Chem. Soc., Dalton Trans.* **1997**, 2639.

(35) (a) Baerlocher, Ch.; Meier, W. M.; Olson, D. H. *Atlas of Zeolite Framework Types*; Elsevier: New York, 2001. (b) Database of Zeolite Structures. http://www.iza-structure.org/databases (accessed Nov 2009).

(36) (a) Chen, C.; Liu, Y.; Fang, Q.; Liu, L.; Eubank, J. F.; Zhang, N.; Gong, S.; Pang, W. *Microporous Mesoporous Mater.* **2006**, *97*, 132. (b) Mandal, S.; Banerjee, D.; Bhat, S. V.; Pati, S. K.; Natarajan, S. *Eur. J. Inorg. Chem.* **2008**, *9*, 1386. (c) Rao, V. K.; Green, M. A.; Pati, S. K.; Natarajan, S. *J. Phys. Chem. B* **2007**, *111*, 12700.

(37) (a) Loiseau, T.; Beitone, L.; Millange, F.; Taulelle, F.; O'Hare, D.; Ferey, G. *J. Phys. Chem. B* **2004**, *108*, 20020. (b) Norquist, A. J.; O'Hare, D. *J. Am. Chem. Soc.* **2004**, *126*, 6673. (c) Walton, R. I.; Norquist, A.; Smith, R. I.; O'Hare, D. *Faraday Discuss.* **2003**, *122*, 331.

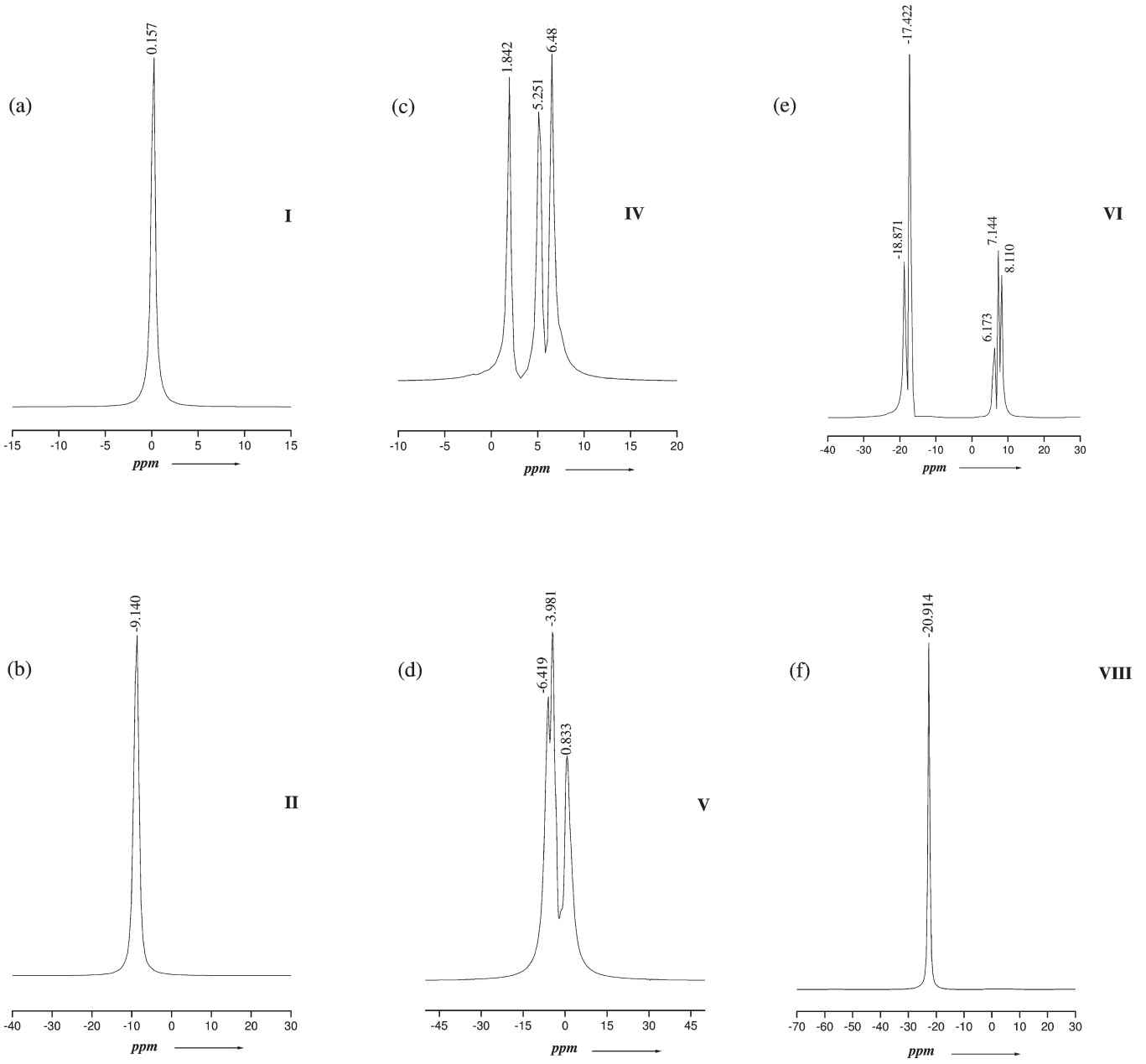


**Figure 14.** $^{31}$P-CPMAS NMR spectra for (a) **I**, (b) **II**, (c) **IV**, (d) **V**, (e) **VI**, and (f) **VIII**.

independent phosphorus species. Thus, for **I**, **II**, and **VIII**, single $^{31}$P signals were observed at +0.157, −9.140, and −20.914 ppm, respectively; three signals for **IV** and **V** at 1.842, 5.251, and 6.481 ppm and −6.419, −3.981, and 0.833 ppm respectively; and five signals for **VI** at −18.871, −17.422, 6.173, 7.144, and 8.110 ppm (Figure 14a−f). Each signal was also accompanied by a set of spinning side bands. As P−O−P linkages are absent, the internuclear distances among the P sites in all of the compounds are similar, and hence the magnitude of the $^{31}$P−$^{31}$P dipole coupling constants could be comparable. The two-dimensional double-quantum or exchange-based NMR studies may not be helpful in the assignment of the respective phosphorus species from the NMR studies alone. The assignment of the individual $^{31}$P spectra can be rationalized by combining the $^{31}$P isotropic chemical shift with the bond distances obtained from the single-crystal structural data.

It has been postulated that as the bond strength of the P−O bond increases, the isotropic chemical shifts of the corresponding phosphorus atom shifts toward the upfield region.[38] The bond valence sum method of Brown[39] can be employed to calculate the bond strengths of the various P−O bonds and correlated with the $^{31}$P spectra. Thus, for **IV**, the bond valence sums of the oxygens, $\sum[S(O^{2-})]$, bonded with the phosphorus atoms, P(1), P(2), and P(3), are 5.477, 5.512, and 5.093, respectively (Table S6, Supporting Information). The observed $^{31}$P peaks at 5.251, 1.842, and 6.481 ppm may correspond to P(1), P(2), and P(3), respectively (Table S7, Supporting Information). A similar trend is also observed in **V**. The valence sum values

(38) (a) Cheetham, A. K.; Clayden, N. J.; Dobson, C. M.; Jakeman, R. J. B. *J. Chem. Soc., Chem. Commun.* **1986**, *3*, 195. (b) Tang, M.-F.; Liu, Y.-H.; Chang, P.-C.; Liao, Y.-C.; Kao, H.-M.; Lii, K.-H. *Dalton Trans.* **2007**, *40*, 4523.
(39) Brown, I. D.; Altermatt, D. *Acta Crystallogr.* **1985**, *B41*, 244.

of 6.165, 5.644, and 7.168 for P(1), P(2), and P(3) may correspond to the $^{31}$P spectra observed at −3.981, +0.833, and −6.419 ppm, respectively. From this, one can surmise that the chemical shifts in the $^{31}$P spectra shift toward more negative values as the bond strength values of the oxygens increase. To validate this, we can check the NMR chemical shifts in compound **VI**, where there are five crystallographically distinct phosphorus atoms. The calculated bond strength values for the oxygen atoms bound to P(1), P(2), P(3), P(4), and P(5) are 5.784, 5.619, 5.598, 5.826, and 6.607, respectively. The observed NMR peaks corresponding to these bond valence sum values would be at +6.173, +7.144, +8.110, −17.422, and −18.871 ppm. Thus, one can combine the bond strength values for assigning the chemical shift values observed in the $^{31}$P NMR spectra unambiguously.

In compounds **I**, **II**, and **VIII**, the bond valence sum of the oxygen atoms bound to the phosphorus atoms are 4.952, 6.109, and 6.917. The NMR peaks are also correspondingly shifted toward the upfield region and are observed at +0.157, −9.140, and −20.914 ppm, respectively.

## Conclusions

The synthesis, structure, and reactivity studies of a family of inorganic−organic hybrid compounds based on indium have been accomplished. Of the eight compounds prepared during the present study, the formation of a molecular zero-dimensional compound and the observation of concomitant polymorphs are noteworthy. The oxalate units in the present compounds exhibit two distinct characteristics: (i) satisfaction of the coordination requirements of In and also provision of the necessary charge balance for the structure and (ii) the *in-plane* and *out-of-plane* connectivity required to extend the dimensionality of the structure. The observation of terminal oxalate units in some of the synthesized compounds suggests that they could be intermediates. The transformation studies on the molecular compound indicate the formation of one of the polymorphs in the presence of pyridine (base) and a pillared layered indium phosphite in the presence of $H_3PO_3$ (acid). This suggests that the molecular hybrid is amenable as a reactive species under both acidic as well as basic conditions. The present study clearly establishes the versatility of the oxalate unit as a network-former in the amine-templated system of compounds.

**Acknowledgment.** S.N. thanks the Department of Science and Technology (DST) and the Council of Scientific and Industrial Research (CSIR), Government of India, for the award of a research grant. S.N. also thanks the Department of Science and Technology (DST), Government of India, for the award of a RAMANNA fellowship. The authors thank Dr. Sukhendu Mandal for useful suggestions on the manuscript. We thank Mr. Ravi, NMR center, IISc for help with the collection of NMR data.

**Supporting Information Available:** Hydrogen-bond interactions in compounds **I**−**VIII**, details of CHN analysis, selected bond angles and distances, crystal data and structure refinement parameters for compound **T1**, table for phosphorus−oxygen bond lengths and the calculated bond strengths (S) at phosphorus and at oxygen in the compounds **I**−**VIII**, table for the assignment of the observed NMR peaks in compounds **I**−**VIII**, figures showing the T-atom connectivity in compounds **II** and **III**, IR spectra, simulated and experimental XRD patterns of compounds, TGA curves, schematic representations of the formation of compounds **III** and **VI**, ORTEP plots for compounds **I**−**VIII** and **T1**, and details of the Boltzmann distribution model. This material is available free of charge via the Internet at http://pubs.acs.org.